Available online at www.sciencedirect.com
ScienceDirect
Journal of Sound and Vibration 321 (2009) 79–103
JOURNAL OF SOUND AND VIBRATION
www.elsevier.com/locate/jsvi

Damping of rotor conical whirl by asymmetric dry friction suspension

Francesco Sorge*

Dipartimento di Meccanica, Università di Palermo, Viale delle Scienze, 90128 Palermo, Italy

Received 25 March 2008; received in revised form 5 August 2008; accepted 9 September 2008
Handling Editor: C.L. Morfey
Available online 23 October 2008

Abstract

A new technique for the rotor whirl damping in rotating machinery, based on the elastic suspension of the journal boxes and the use of dry friction surfaces normal to the shaft axis between their supports and the frame, is here analysed theoretically for several cases of rotor systems characterized by mass and constraint asymmetry, where gyroscopic effects are to be expected and conical whirl motions may grow up. The critical flexural speeds can be easily cut off by an adhesive state of the supports and the whirl amplitude can be minimized as well throughout the remaining sliding range. Confining the operative angular speed of the rotor in the range of adhesive contact between the dry friction surfaces, no significant increase of power dissipation or heat production has to be ascribed as a whole to this type of suspension system, whose task is just to suppress the resonant peaks when passing the critical speeds. On the other hand, the rubbing surface wear can be easily compensated in the long run by use of suitable spring devices to close the friction contact. The uniqueness and the stability of the steady motion are proved, both in the absence and in the presence of possible additional viscous sources of dissipation. It is also shown how the destabilizing influence of the shaft material hysteresis can be counterbalanced by the other external dissipative forces.

1. Introduction

Even a small mass unbalance may generate violent and dangerous whirling motions of a rotor on approaching critical flexural speeds, which are known to be in close correlation with the elastic and inertial characteristics of the machine. Annular motion-limiting stops or squeeze-film dampers may restrain the whirling motions [1–6], introducing a certain level of physical and/or geometrical nonlinearity into the whirl model, together with the possible onset of instability conditions or non-synchronous oscillations.

Setting up compliant supports may improve the frequency response, but the number of degrees of freedom and critical speeds increases and wider speed ranges are to be controlled to prevent undesired critical conditions. Flexible damped supports have been widely analysed in the past (see for example [7–12]), showing a behaviour more or less similar to the viscously damped dynamical vibration absorbers, and even gas bearing

*Tel.: +39 091 6657157; fax: +39 091 6657163.
E-mail address: sorge@dima.unipa.it

0022-460X/$ - see front matter © 2008 Elsevier Ltd. All rights reserved.
doi:10.1016/j.jsv.2008.09.009

Nomenclature (dimensionless quantities unless specified)

$\mathbf{A}$, $\mathbf{A}_0$ flexibility matrices for moving support and fixed-support systems
c_t, c_r, c_h translational (N s/m), rotational (N s m) and hysteretic coefficients of damping (N s/m)
c_{ij} inversion coefficients of impedance matrix $\mathbf{Z}$
d_t, d_r translational and rotational damping factors
d_h hysteretic factor
$\mathbf{D}$ damping matrix
e rotor eccentricity (m)
E Young's modulus (N/m^2)
$\mathbf{F}_h$ hysteretic force on rotor (N)
$\mathbf{F}_{xz}$, $\mathbf{F}_{yz}$ force–moment vectors on bending planes xz and yz
$G = mg/(ek)$ dimensionless gravity field
$\mathbf{H}$ hysteresis matrix
I moment of inertia of shaft cross-section (m^4)
j_d, j_a diametral and axial moment of inertia of rotor (kg m^2)
$J_d = j_d/(ml^2)$, $J_a = j_a/(ml^2)$ dimensionless diametral and axial moment of inertia of rotor
k reference shaft stiffness (N/m)
k_3, k_4 suspension stiffness (N/m)
$\mathbf{K}$ stiffness matrix
$K_3 = k_3/k$, $K_4 = k_4/k$ dimensionless suspension stiffness
l shaft length (m)
L Lyapunov function
$L_3 = -z_3/l$, $L_4 = z_4/l$ dimensionless distances of rotor from supports
m rotor mass (kg)
m_3, m_4 support mass (kg)
$\mathbf{M}$ mass matrix
$M_3 = m_3/m$, $M_4 = m_4/m$ dimensionless support mass
$\hat{N}_3, \hat{N}_4$ friction phasors (scaled by sliding force amplitudes)
R_1, R_2, R_3, R_4 dimensionless whirling amplitudes of rotor path (1) and tilt (2) and of support paths (3) and (4)
$\mathbf{v}_{\text{rel.}}$ relative velocity vector (m/s)
$\mathbf{V}$ dimensionless velocity vector
$\mathbf{w}_0$ complex amplitude vector of natural modes (m)
$\mathbf{W}(\theta)$, $\mathbf{\Delta W}(\theta)$ complex displacement–rotation vector, difference between two solutions
$\mathbf{W}_0$ complex amplitude vector of steady whirling
x, y, z, x_0, y_0, z_0 coordinates in non-rotating references (m)
$\mathbf{X}$, $\mathbf{Y}$ displacement–rotation vectors
$\mathbf{Z}$ complex impedance matrix
α angle between steady and perturbed velocities
γ_1, γ_2, γ_3, γ_4 angular phases of rotor path (1) and tilt (2) and of support paths (3) and (4)
$\theta = \omega t$ angular rotation variable
$\lambda = \omega_n/\omega$ ratio of natural whirling speed to shaft speed
ξ, η, ζ, ξ_0, η_0, ζ_0 coordinates in rotating references (m)
σ (= 1 or 0) sliding or adhesion indicator
φ, ψ small rotation angles around x and y due to shaft bending
$\boldsymbol{\phi}$, $\boldsymbol{\phi}_{\text{adh.}}$ sliding and adhesion friction forces (N)
$\Phi = \phi/(ek)$, $\Phi_{\text{adh.}} = \phi_{\text{adh.}}/(ek)$ dimensionless sliding and adhesion friction forces
$\hat{\Phi}_{\text{adh.}}$ dimensionless complex adhesion force
ω angular speed (s^{-1})
$\omega_c = k/m$ reference critical speed (s^{-1})
$\Omega = \omega/\omega_c$ dimensionless angular speed
$\Omega_n = \omega_n/\omega_c$ dimensionless whirling speed in natural mode

Subscripts and superscripts

(c) cofactor matrix
r, i real, imaginary
r, t rotational and translational damping
T transpose matrix
real real matrix
1 rotor centre displacement
2 rotor tilt
3 back support displacement
4 front support displacement
* inversion auxiliary matrices (Section 6)
$(\ldots)'$, $(\ldots)''$ first, second derivative with respect to θ
$\widetilde{(\ldots)}$ perturbation variable

suspension systems have been studied and applied in high-speed turbomachines [13–15]. Nevertheless, a drawback of the viscous suspension is the introduction of a source of dissipation that remains active also at the nominal operating point, even far from the critical speeds.

The present analysis originates from the idea of suspending the shaft journal boxes on suitable springs and creating, on the supports, flat rubbing surfaces orthogonal to the shaft axis, with the function of damping the critical whirling motion by dry friction. A previous study has ascertained the feasibility of this technique for a symmetric rotor of the Laval–Jeffcott type with symmetric side constraints, by an in-depth dynamical analysis throughout the whole speed range [16]. Here, a more general typology will be approached, where the symmetry with respect to the mid-plane is removed and gyroscopic effects intervene to complicate the rotor response. The uniqueness and stability of the steady motion will be carefully studied also for these cases, considering the shaft internal hysteresis as well.

It is noteworthy that the wear compensation of sliding surfaces may be made automatic by using suitable spring devices to load the friction pads (e.g. Belleville washers or other springs). Moreover, it is remarkable that the sliding condition between the friction surfaces may be rendered infrequent enough in practice if an adhesive contact state is suitably planned for an extended portion of the speed range and this motionless support configuration is chosen for the usual working condition of the rotating machine, while the sliding operation is programmed to start spontaneously to choke the whirling motion when passing occasionally through what would be a critical speed of the fixed-support system. The advantage of dry friction dampers consists thus in that they behave similar to clutches, which either lock or release the connection between the journal boxes and the frame depending on the rotational speed, in such a way that, during the normal operative conditions, there is neither power dissipation nor heat production because the friction devices are motionless. This behaviour can be achieved by a proper choice of the friction level in dependence on the suspension-to-shaft stiffness ratios and on the support-to-rotor mass ratios.

The dry friction application in rotating machinery was claimed by some patents in the past [17,18], but there was not a thorough analysis of the dynamical behaviour of this support configuration.

2. Mathematical model

The compliant side supports subject to dry friction introduce a strong nonlinearity due to the continuous self-alignment of the friction forces on the one and the other support in opposition to the variable directions of the instantaneous sliding velocities. Yet, in the hypothesis of equal stiffness of each single suspension and of the shaft in the one and the other transversal direction, a steady-state rotating solution may be obtained straightforwardly in closed form.

Fig. 1 describes the dynamical system under examination and may be used as a reference for the notation. The point of view of the present theoretical approach is similar to that of Refs. [19,20]. It is supposed that the mass centre C is placed at a fixed distance e from the intersection O_1 of the shaft axis with the rotor diametral plane. The frame $Cxyz$ moves with C remaining parallel to the fixed frame $Ox_0y_0z_0$, while the frame $C\xi\eta\zeta$ is a particular principal frame of the rotor, obtainable by another principal frame fixed to the rotor itself, by means of a backward rotation of the diametral axes ξ and η around ζ through the rotor rotation angle $\theta = \omega t$. Then, the reference $C\xi\eta\zeta$ does not take part in the main rotating motion with angular speed ω, but only performs small rotations φ and ψ around axes x and y because of the shaft elastic deformation. Furthermore, the direction of y_0 and y is chosen opposite to the gravitational field $\mathbf{g}$.

Some external environmental dissipation is supposed to act on the rotor translational and rotational motions, due for example to the gas or the steam flowing through the rotating blades if a turbomachine is being considered. These aerodynamic resistances are assumed viscous-like (linear) for simplicity and the viscous equivalent coefficients c_t (N s/m) and c_r (N s m) are introduced in correspondence.

The internal dissipative force on the rotor due to the shaft hysteresis is correlated, similar to [16], with the velocity $\mathbf{v}_{\text{rel.}}$ of the rotor centre O_1 relative to a reference system $O_3\xi_0\eta_0\zeta_0$ having the coordinate axis ζ_0 through the centres of the shaft end sections and rotating rigidly with such end sections at the same angular speed ω (detail of Fig. 1). In the case of a shaft on two supports, define $L_3 = -z_3/l$ and $L_4 = z_4/l$ the dimensionless distances of the rotor from the shaft ends, where l is the shaft length. Components of $\mathbf{v}_{\text{rel.}}$ in the fixed reference $Ox_0y_0z_0$ are given by $v_{\text{rel.},x} = \dot{x}_1 - \dot{x}_3L_4 - \dot{x}_4L_3 + \omega(y_1 - y_3L_4 - y_4L_3)$ and

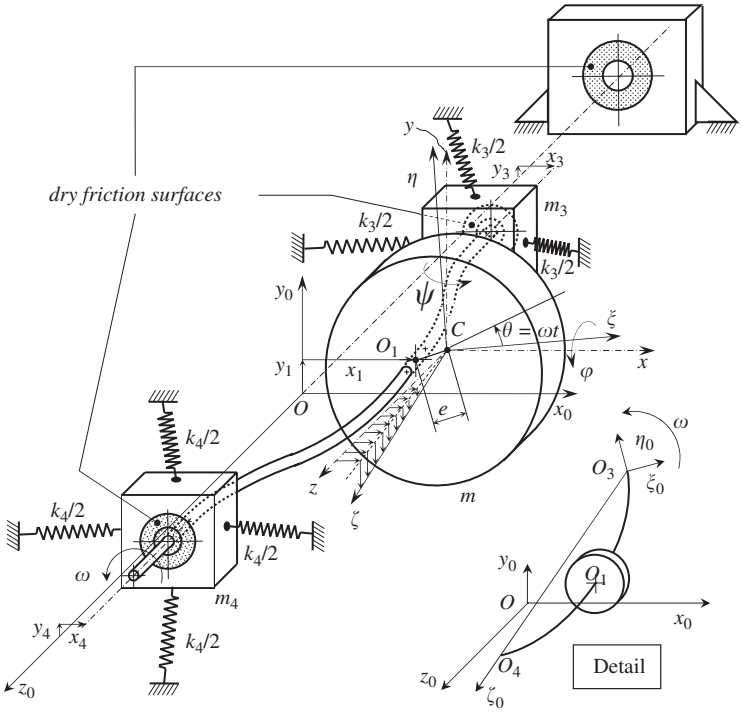

Fig. 1. Scheme of rotating machine with expanded view of back support and frame. Detail: reference system rotating with end sections.

$v_{\mathrm{rel.},y} = \dot{y}_1 - \dot{y}_3 L_4 - \dot{y}_4 L_3 - \omega(x_1 - x_3 L_4 - x_4 L_3)$, while for a cantilever shaft clamped at 3 and loaded at 4, they are $v_{\mathrm{rel.},x} = \dot{x}_1 - \dot{x}_3 + \omega(y_1 - y_3)$ and $v_{\mathrm{rel.},y} = \dot{y}_1 - \dot{y}_3 - \omega(x_1 - x_3)$. The hysteresis force on the rotor, opposite to the relative velocity of O_1, is obtained multiplying this velocity by a hysteretic coefficient c_h: $\mathbf{F}_h = -c_h \mathbf{v}_{\mathrm{rel.}}$. The corresponding forces on the two supports are calculated imposing the vanishing of the resultant moment of the hysteretic forces on the rotor, $\mathbf{F}_{3h} = -L_4 \mathbf{F}_h$, $\mathbf{F}_{4h} = -L_3 \mathbf{F}_h$, or otherwise one has $\mathbf{F}_{3h} = -\mathbf{F}_h$ in the case of a cantilever shaft.

The torsional deformation between the rotor and the end sections is ignored, because any possible torsional oscillation is uncoupled with the bending motion. Moreover, the shaft mass is neglected (Jeffcott rotor assumption).

Introducing the angular time variable $\theta = \omega t$, the differentiation with respect to θ is indicated with primes, whence $\mathrm{d}(\ldots)/\mathrm{d}t = \omega(\ldots)'$, etc. Indicating with k the reference shaft stiffness, which may be taken from the symmetric case with fixed support (e.g. $k = 48EI/l^3$ for self-aligning bearings or $k = 192EI/l^3$ for cylindrical bearings), and with $\omega_c = \sqrt{k/m}$ the reference critical speed, the angular speed ratio $\Omega = \omega/\omega_c$, the mass ratios, $M_3 = m_3/m$ and $M_4 = m_4/m$, the stiffness ratios, $K_3 = k_3/k$ and $K_4 = k_4/k$, are also introduced. Moreover, the damping factors $d_t = 0.5 c_t \omega_c/k$ and $d_r = 0.5 c_r \omega_c/(kl^2)$ are introduced for the translational and rotational motions and the dimensionless acceleration of gravity $G = mg/ek$ is used to account for the weight.

As well known, in steady conditions, one of the effects of gravity is that the whole shaft does not rotate rigidly with its bending plane and supports, with some rotor shift due to the unbalance, but point O_1 travels along a circular path, with respect to the rotating reference frame $O_3\xi_0\eta_0\zeta_0$ of Fig. 1, counter-rotating with the angular speed $-\omega$. Therefore, assuming the hysteretic work proportional to the cycle area, i.e. assuming that the integral $c_h \oint (v^2_{\mathrm{rel.},x} + v^2_{\mathrm{rel.},y})\,\mathrm{d}t = c_h \omega \oint [(x_1' - L_4 x_3' - L_3 x_4' + y_1 - L_4 y_3 - L_3 y_4)^2 + (y_1' - L_4 y_3' - L_3 y_4' - x_1 + L_4 x_3 + L_3 x_4)^2]\,\mathrm{d}\theta$ is proportional to the square of the path radius independent of ω, it is easy to conclude that the product $c_h\omega$ may be considered constant on varying ω, whence a constant hysteresis factor $d_h = 0.5 c_h \omega/k$ is here introduced (see [21]).

In sliding conditions, it is assumed that the total friction force vectors $\boldsymbol{\phi}_3$ and $\boldsymbol{\phi}_4$ have constant amplitudes and are opposite to the support translational velocities. Therefore, components of these forces are $-\phi_j x'_j/\sqrt{x'^2_j + y'^2_j}$ and $-\phi_j y'_j/\sqrt{x'^2_j + y'^2_j}$ (for $j = 3, 4$). In the case of stuck condition of any of the two supports, the sliding force $\boldsymbol{\phi}_j$ has to be replaced by an adhesive force $\boldsymbol{\phi}_{\mathrm{adh},j}$, which is not known a priori, but must balance the other forces on the support. The magnitude of all these friction forces may be made dimensionless by introducing the friction variables $\Phi_j = \phi_j/(ke)$ and $\Phi_{\mathrm{adh.},j} = \phi_{\mathrm{adh},j}/(ke)$.

In view of a complete dimensionless formulation, all displacements are scaled by the rotor eccentricity e and all rotations by e/l, so that, using capital letters for the dimensionless quantities and assigning the subscripts 1 and 2 to the rotor displacement and tilt, the following dimensionless displacement–rotation vectors are introduced

$$\mathbf{X} = \{X_1, X_2, X_3, X_4\}^{\mathrm{T}}, \quad \mathbf{Y} = \{Y_1, Y_2, Y_3, Y_4\}^{\mathrm{T}} \tag{1}$$

where $X_j = x_j/e$, $Y_j = y_j/e$, for $j \neq 2$, $X_j = \psi l/e$, $Y_j = -\varphi l/e$, for $j = 2$, and the subscript j refers to the rotor displacement ($j = 1$), or to the rotations around y and x ($j = 2$), or to the support displacements ($j = 3, 4$). Notice that the sign of rotation φ around x-axis was changed, when introducing the dimensionless rotation Y_2, in order to use the same flexibility (or stiffness) matrix for both the bending planes, xz and yz.

Taking into account the gyroscopic effects in the evaluation of the total moment of the inertia forces with respect to the mass centre, the dimensionless force–moment expressions in the bending planes xz and yz may be written in the vector form:

$$\begin{aligned}\mathbf{F}_{xz} = &-\Omega^2\begin{Bmatrix} X''_1 - \cos\theta \\ J_d X''_2 + J_a Y'_2 \\ M_3 X''_3 \\ M_4 X''_4 \end{Bmatrix} - 2\Omega\begin{Bmatrix} d_t X'_1 \\ d_r X'_2 \\ 0 \\ 0 \end{Bmatrix} - 2d_h\begin{Bmatrix} X'_1 + Y_1 - L_4(X'_3 + Y_3) - L_3(X'_4 + Y_4) \\ 0 \\ -L_4(X'_1 + Y_1) + L_4^2(X'_3 + Y_3) + L_3L_4(X'_4 + Y_4) \\ -L_3(X'_1 + Y_1) + L_3L_4(X'_3 + Y_3) + L_3^2(X'_4 + Y_4) \end{Bmatrix} \\ &- \begin{Bmatrix} 0 \\ 0 \\ \dfrac{\sigma_3\Phi_3 X'_3}{\sqrt{X'^2_3 + Y'^2_3}} + (1-\sigma_3)\Phi_{\mathrm{adh.3},x} \\ \dfrac{\sigma_4\Phi_4 X'_4}{\sqrt{X'^2_4 + Y'^2_4}} + (1-\sigma_4)\Phi_{\mathrm{adh.4},x} \end{Bmatrix}\end{aligned} \tag{2a}$$

$$\begin{aligned}\mathbf{F}_{yz} = &-\Omega^2\begin{Bmatrix} Y''_1 - \sin\theta \\ J_d Y''_2 - J_a X'_2 \\ M_3 Y''_3 \\ M_4 Y''_4 \end{Bmatrix} - 2\Omega\begin{Bmatrix} d_t Y'_1 \\ d_r Y'_2 \\ 0 \\ 0 \end{Bmatrix} - 2d_h\begin{Bmatrix} Y'_1 - X_1 - L_4(Y'_3 - X_3) - L_3(Y'_4 - X_4) \\ 0 \\ -L_4(Y'_1 - X_1) + L_4^2(Y'_3 - X_3) + L_3L_4(Y'_4 - X_4) \\ -L_3(Y'_1 - X_1) + L_3L_4(Y'_3 - X_3) + L_3^2(Y'_4 - X_4) \end{Bmatrix} \\ &- \begin{Bmatrix} 0 \\ 0 \\ \dfrac{\sigma_3\Phi_3 Y'_3}{\sqrt{X'^2_3 + Y'^2_3}} + (1-\sigma_3)\Phi_{\mathrm{adh.3},y} \\ \dfrac{\sigma_4\Phi_4 Y'_4}{\sqrt{X'^2_4 + Y'^2_4}} + (1-\sigma_4)\Phi_{\mathrm{adh.4},y} \end{Bmatrix} - G\begin{Bmatrix} 1 \\ 0 \\ M_3 \\ M_4 \end{Bmatrix}\end{aligned} \tag{2b}$$

where for $j = 1, 3, 4$, $F_{xz,j}$ and $F_{yz,j}$ refer to x-components and y-components of the forces applied to the rotor ($j = 1$) and to the supports ($j = 3, 4$), while for $j = 2$, $F_{xz,j}$ and $-F_{yz,j}$ give y- and x-component of the moment acting on the rotor. All forces are scaled by ke, all moments by kel and each of the coefficients σ_3 and σ_4 has to be set equal either to 1 or to 0, depending on the slip or stick condition of the supports 3 and 4, respectively. Moreover, $J_d = j_d/ml^2$ and $J_a = j_a/ml^2$ are the dimensionless diametral and axial moment of inertia of the rotor, scaled by the product ml^2, where j_d and j_a are the real moment of inertia. The force vectors were split, in Eq. (2), in their distinct components, inertial, viscous, hysteretic, coulombian and gravitational.

According to the form chosen for the displacement–rotation and force–moment vectors, introduce the following dimensionless flexibility matrix:

$$\mathbf{A} = \begin{bmatrix} A_{0,11} + \dfrac{L_4^2}{K_3} + \dfrac{L_3^2}{K_4} & A_{0,12} - \dfrac{L_4}{K_3} + \dfrac{L_3}{K_4} & \dfrac{L_4}{K_3} & \dfrac{L_3}{K_4} \\ A_{0,21} - \dfrac{L_4}{K_3} + \dfrac{L_3}{K_4} & A_{0,22} + \dfrac{1}{K_3} + \dfrac{1}{K_4} & -\dfrac{1}{K_3} & \dfrac{1}{K_4} \\ \dfrac{L_4}{K_3} & -\dfrac{1}{K_3} & \dfrac{1}{K_3} & 0 \\ \dfrac{L_3}{K_4} & \dfrac{1}{K_4} & 0 & \dfrac{1}{K_4} \end{bmatrix} \tag{3}$$

where the shaft flexibility sub-matrix 2×2 $[A_0]$ is evaluated under the hypothesis of fixed supports. For example, for self-aligning bearings (hinged–hinged beam) and for cylindrical bearings (clamped–clamped beam), one has, respectively,

$$\begin{aligned} \text{self-aligning} : \mathbf{A}_0 &= 16 \begin{bmatrix} L_3^2 L_4^2 & L_3 L_4 (L_4 - L_3) \\ L_3 L_4 (L_4 - L_3) & 1 - 3 L_3 L_4 \end{bmatrix} \\ &= k \begin{bmatrix} 1 & 0 \\ 0 & l \end{bmatrix} \begin{bmatrix} l^3 L_3^2 L_4^2/(3EI) & l^2 L_3 L_4 (L_4 - L_3)/(3EI) \\ l^2 L_3 L_4 (L_4 - L_3)/(3EI) & l(1 - 3 L_3 L_4)/(3EI) \end{bmatrix} \begin{bmatrix} 1 & 0 \\ 0 & l \end{bmatrix} \end{aligned} \tag{4a}$$

$$\begin{aligned} \text{cylindrical} : \mathbf{A}_0 &= 192 \begin{bmatrix} L_3^3 L_4^3/3 & L_3^2 L_4^2 (L_4 - L_3)/2 \\ L_3^2 L_4^2 (L_4 - L_3)/2 & L_3 L_4 (L_3 + L_4 - 3 L_3 L_4) \end{bmatrix} \\ &= k \begin{bmatrix} 1 & 0 \\ 0 & l \end{bmatrix} \begin{bmatrix} l^3 L_3^3 L_4^3/(3EI) & l^2 L_3^2 L_4^2 (L_4 - L_3)/(2EI) \\ l^2 L_3^2 L_4^2 (L_4 - L_3)/(2EI) & l L_3 L_4 (L_3 + L_4 - 3 L_3 L_4)/(EI) \end{bmatrix} \begin{bmatrix} 1 & 0 \\ 0 & l \end{bmatrix} \end{aligned} \tag{4b}$$

At last, a symmetric hysteretic matrix $\mathbf{H}$ can be defined:

$$\mathbf{H} = d_h \begin{bmatrix} 1 & 0 & -L_4 & -L_3 \\ 0 & 0 & 0 & 0 \\ -L_4 & 0 & L_4^2 & L_3 L_4 \\ -L_3 & 0 & L_3 L_4 & L_3^2 \end{bmatrix} \tag{5}$$

and accounting for Eqs. (1)–(5), the equations of motion, $\mathbf{X} - \mathbf{A}\mathbf{F}_{xz} = 0$, $\mathbf{Y} - \mathbf{A}\mathbf{F}_{yz} = 0$, turn out to be

$$\mathbf{K}\mathbf{X} + 2\Omega\mathbf{D}\mathbf{X}' + 2\mathbf{H}(\mathbf{X}' + \mathbf{Y}) + \Omega^2\mathbf{M}\mathbf{X}'' + \begin{Bmatrix} -\Omega^2 \cos\theta \\ \Omega^2 J_a Y_2' \\ \sigma_3 \Phi_3 X_3' \Big/ \sqrt{X_3'^2 + Y_3'^2} + (1 - \sigma_3)\Phi_{\text{adh.3},x} \\ \sigma_4 \Phi_4 X_4' \Big/ \sqrt{X_4'^2 + Y_4'^2} + (1 - \sigma_4)\Phi_{\text{adh.4},x} \end{Bmatrix} = 0 \tag{6a}$$

$$\mathbf{KY}+2\Omega\mathbf{DY}'+2\mathbf{H}(\mathbf{Y}'-\mathbf{X})+\Omega^2\mathbf{MY}''+\left\{\begin{array}{c}-\Omega^2\sin\theta+G\\ -\Omega^2 J_a X'_2\\ \sigma_3\Phi_3 Y'_3\Big/\sqrt{X'^2_3+Y'^2_3}+(1-\sigma_3)\Phi_{\mathrm{adh}.3,y}+GM_3\\ \sigma_4\Phi_4 Y'_4\Big/\sqrt{X'^2_4+Y'^2_4}+(1-\sigma_4)\Phi_{\mathrm{adh}.4,y}+GM_4\end{array}\right\}=0 \tag{6b}$$

where $\mathbf{K}=\mathbf{A}^{-1}$ is the stiffness matrix and $\mathbf{D}$ and $\mathbf{M}$ are the viscous and mass matrices, which are diagonal with coefficients (d_t, d_r, 0, 0) and (1, J_d, M_3, M_4), respectively.

The constant part of the solution, i.e. the central equilibrium configuration of the rotor, can be easily obtained by Eq. (6), though this solution must not be considered unique, as will be better specified in the following, because the adhesive condition between the friction surfaces can be satisfied in an infinite number of positions, provided that the static friction limit is not attained. One has, for zero adhesive force,

$$\mathbf{X}_{\mathrm{equil.}}=-2\mathbf{AHY}_{\mathrm{equil.}},\quad \mathbf{Y}_{\mathrm{equil.}}=2\mathbf{AHX}_{\mathrm{equil.}}-G\mathbf{A}\{1,0,M_3,M_4\}^{\mathrm{T}} \tag{7}$$

and as $\mathbf{X}_{\mathrm{equil.}}\neq 0$, the well-known static bias due to hysteresis is observable.

In the case of a cantilever shaft, for example clamped at the support 3 and carrying the rotor at the free end 4, all the above vectors and matrices become three dimensional and, assuming $k=3EI/l^3$ as the reference shaft stiffness, matrices $\mathbf{A}$ and $\mathbf{H}$ are given by

$$\mathbf{A}=\begin{bmatrix}1+\frac{1}{K_3} & \frac{3}{2} & \frac{1}{K_3}\\ \frac{3}{2} & 3 & 0\\ \frac{1}{K_3} & 0 & \frac{1}{K_3}\end{bmatrix},\quad \mathbf{H}=d_h\begin{bmatrix}1 & 0 & -1\\ 0 & 0 & 0\\ -1 & 0 & 1\end{bmatrix} \tag{8a,b}$$

where the dimensionless flexibility sub-matrix $\mathbf{A}_0=\begin{bmatrix}1 & 3/2\\ 3/2 & 3\end{bmatrix}$ has been used. The central equilibrium configuration is still given by Eq. (7), using the mass vector $\{1,\ 0,\ M_3\}^{\mathrm{T}}$.

In case of adherence of any support (i.e. if $\sigma_j=0$, for $j=3$ or/and 4), an infinite number of other equilibrium solutions may be found. They can be obtained by Eq. (7) adding $A_{ij}\Phi_{\mathrm{adh}.j,\,x,\,\mathrm{eq.}}$ to $X_{i,\mathrm{equil.}}$, and adding $A_{ij}\Phi_{\mathrm{adh}.j,\,y,\,\mathrm{eq.}}$ to $Y_{i,\mathrm{equil.}}$, where the values of $\Phi_{\mathrm{adh}.j,\,x,\,\mathrm{eq.}}$ and $\Phi_{\mathrm{adh}.j,\,y,\,\mathrm{eq.}}$ are arbitrary at all, provided that the static friction limit is not exceeded. Thus, such positions may be imagined as reachable by a rigid displacement from the reference configuration, $\Phi_{\mathrm{adh}.j,\,x,\,\mathrm{eq.}}=\Phi_{\mathrm{adh}.j,\,y,\,\mathrm{eq.}}=0$ of Eq. (7) and absorb the constant amounts $\Phi_{\mathrm{adh}.j,\,x,\,\mathrm{eq.}}$ and $\Phi_{\mathrm{adh}.j,\,y,\,\mathrm{eq.}}$ of the total adhesive forces. Anyway, on varying the angular speed smoothly and continuously and passing from the quasi-steady sliding to the sticking state, the journal box position tends to the central configuration of Eq. (7), as will be seen in the following, and moreover, even a hypothetical different position would not affect the rotor motion around it at all. Therefore, it will be assumed that $\Phi_{\mathrm{adh}.j,\,x,\,\mathrm{eq.}}=\Phi_{\mathrm{adh}.j,\,y,\,\mathrm{eq.}}=0$ and, from now onward, the vectors $\mathbf{X}$ and $\mathbf{Y}$ will be assumed curtailed of their constant content, as if the gravity effects were absent (e.g. vertical shaft).

The dynamic remainder of the differential system (6a,b) can be further compacted multiplying Eq. (6b) by the unit imaginary number i, summing it to Eq. (6a) and putting $\mathbf{W}=\mathbf{X}+\mathrm{i}\mathbf{Y}$, $\hat{\Phi}_{\mathrm{adh}.j}=\Phi_{\mathrm{adh}.j,\,x}+\mathrm{i}\Phi_{\mathrm{adh}.j,\,y}$:

$$\mathbf{KW}+2\Omega\mathbf{DW}'+2\mathbf{H}(\mathbf{W}'-\mathrm{i}\mathbf{W})+\Omega^2\mathbf{MW}''+\left\{\begin{array}{c}-\Omega^2\exp(\mathrm{i}\theta)\\ -\mathrm{i}\Omega^2 J_a W'_2\\ \sigma_3\Phi_3\exp(\mathrm{i}\arg W'_3)+(1-\sigma_3)\hat{\Phi}_{\mathrm{adh}.3}\\ \sigma_4\Phi_4\exp(\mathrm{i}\arg W'_4)+(1-\sigma_4)\hat{\Phi}_{\mathrm{adh}.4}\end{array}\right\}=0 \tag{9}$$

3. Uniqueness of the circular solution

In a following section, a steady-state circularly polarized solution of Eq. (9) will be discussed. Here, uniqueness of this solution will be proved *ad absurdum* for the case of absence of hysteresis and no adhesion ($\sigma_3=\sigma_4=1$). Indicating it with $\mathbf{W}(\theta)_c$, indicating with $\mathbf{W}(\theta)_s$ any other hypothetical steady solution, provided it exists, with period 2π, or else multiple or sub-multiple of 2π, and defining $\mathbf{\Delta W}(\theta)=\mathbf{W}(\theta)_c-\mathbf{W}(\theta)_s$ their difference, the co-existence of such solutions would permit rewriting Eq. (9) as follows:

$$\mathbf{K}\,\mathbf{\Delta W}+2\Omega\mathbf{D}\,\mathbf{\Delta W}'+\Omega^2\mathbf{M}\,\mathbf{\Delta W}''+\{0,\mathrm{i}\Omega^2 J_a(W'_{2s}-W'_{2c}),\Phi_3[\exp(\mathrm{i}\arg W'_{3c})-\exp(\mathrm{i}\arg W'_{3s})],\Phi_4[\exp(\mathrm{i}\arg W'_{4c})-\exp(\mathrm{i}\arg W'_{4s})]\}^{\mathrm{T}}=0 \tag{10}$$

Then, indicating with an overbar and with the notation $\mathrm{Re}(\ldots)$ the complex conjugate and the real part of any complex number, pre-multiplying Eq. (10) by $\mathbf{\Delta\bar{W}'}^{\mathrm{T}}$ and adding it to the complex conjugate of the same equation, pre-multiplied by $\mathbf{\Delta W'}^{\mathrm{T}}$, one obtains

$$\begin{aligned}&2\mathrm{Re}\left(\sum_{i,j}K_{ij}\,\Delta\bar{W}'_i\,\Delta W_j+\Omega^2\sum_j M_{jj}\,\Delta\bar{W}'_j\,\Delta W''_j\right)+4\Omega\sum_j D_{jj}\left|\Delta W'_j\right|^2\\&+\Phi_3\left[\left|W'_{3c}\right|\exp(-\mathrm{i}\arg W'_{3c})-\left|W'_{3s}\right|\exp(-\mathrm{i}\arg W'_{3s})\right]\left[\exp(\mathrm{i}\arg W'_{3c})-\exp(\mathrm{i}\arg W'_{3s})\right]\\&+\Phi_3\left[\left|W'_{3c}\right|\exp(\mathrm{i}\arg W'_{3c})-\left|W'_{3s}\right|\exp(\mathrm{i}\arg W'_{3s})\right]\left[\exp(-\mathrm{i}\arg W'_{3c})-\exp(-\mathrm{i}\arg W'_{3s})\right]\\&+\Phi_4\left[\left|W'_{4c}\right|\exp(-\mathrm{i}\arg W'_{4c})-\left|W'_{4s}\right|\exp(-\mathrm{i}\arg W'_{4s})\right]\left[\exp(\mathrm{i}\arg W'_{4c})-\exp(\mathrm{i}\arg W'_{4s})\right]\\&+\Phi_4\left[\left|W'_{4c}\right|\exp(\mathrm{i}\arg W'_{4c})-\left|W'_{4s}\right|\exp(\mathrm{i}\arg W'_{4s})\right]\left[\exp(-\mathrm{i}\arg W'_{4c})-\exp(-\mathrm{i}\arg W'_{4s})\right]=0\end{aligned} \tag{11}$$

Integrating with respect to θ over any common multiple of the two periods, of $\mathbf{W}(\theta)_c$ and $\mathbf{W}(\theta)_s$, the elastic and the inertia terms would vanish due to the solution periodicity and Eq. (11) would yield

$$\begin{aligned}&4\Omega\sum_j D_j\int_0^{2n\pi}\left|\Delta W'_j\right|^2\mathrm{d}\theta\\&+2\Phi_3\int_0^{2n\pi}\left(\left|W'_{3c}\right|+\left|W'_{3s}\right|\right)\left[1-\cos(\arg W'_{3c}-\arg W'_{3s})\right]\mathrm{d}\theta\\&+2\Phi_4\int_0^{2n\pi}\left(\left|W'_{4c}\right|+\left|W'_{4s}\right|\right)\left[1-\cos(\arg W'_{4c}-\arg W'_{4s})\right]\mathrm{d}\theta=0\end{aligned} \tag{12}$$

In the case of two distinct solutions, $\mathbf{W}(\theta)_c\neq\mathbf{W}(\theta)_s$, the integral of the viscous term would certainly be positive, while the integral of the dry friction terms would be essentially non-negative and would vanish only for constantly equal arguments of the complex sliding velocities of the two solutions, $\arg W'_{3c}\equiv\arg W'_{3s}$, $\arg W'_{4c}\equiv\arg W'_{4s}$, i.e. for constantly aligned sliding velocities. Nevertheless, should this condition be satisfied, even with no viscous dissipation ($\mathbf{D}\equiv 0$), Eq. (10) would produce, for the new vector variable $\mathbf{\Delta W}(\theta)$, the ideal natural solutions of the linear non-dissipative autonomous system, with their own circular frequencies, in contradiction with the hypothesis of velocity parallelism.

Therefore, the steady circular solution is certainly unique in the case of full sliding of both journal boxes and of ideally elastic shaft, while the above proof may no longer hold for sticking journal boxes, where several adhesive solutions may co-exist, as said before, or in presence of hysteresis of the shaft material, in which case, the above procedure implies a hysteretic integral whose positiveness cannot be ascertained. Nevertheless, if the hysteresis effect is slight, the positive integrals of Eq. (12) prevail and the solution is unique as well.

4. Stability

A logic similar to the previous section permits proving the stability of the circular solution for sliding supports, in absence of hysteresis.

Assume that a perturbation characterized by vectors $\tilde{\mathbf{X}}$ and $\tilde{\mathbf{Y}}$ of arbitrary amplitude not necessarily small, is superimposed on the steady solution. Applying Eqs. (6) to the perturbed motion, subtracting then their

expressions for the steady motion and recalling that the only nonlinear terms are the dry friction ones, one can write

$$\mathbf{K}\tilde{\mathbf{X}}+2\Omega\mathbf{D}\tilde{\mathbf{X}}'+\Omega^2\mathbf{M}\tilde{\mathbf{X}}''+\left\{\begin{array}{c}0\\ \Omega^2 J_a\tilde{Y}'_2\\ \Phi_3\left[\dfrac{X'_3+\tilde{X}'_3}{\sqrt{(X'_3+\tilde{X}'_3)^2+(Y'_3+\tilde{Y}'_3)^2}}-\dfrac{X'_3}{\sqrt{X'^2_3+Y'^2_3}}\right]\\ \Phi_4\left[\dfrac{X'_4+\tilde{X}'_4}{\sqrt{(X'_4+\tilde{X}'_4)^2+(Y'_4+\tilde{Y}'_4)^2}}-\dfrac{X'_4}{\sqrt{X'^2_4+Y'^2_4}}\right]\end{array}\right\}=0 \tag{13a}$$

$$\mathbf{K}\tilde{\mathbf{Y}}+2\Omega\mathbf{D}\tilde{\mathbf{Y}}'+\Omega^2\mathbf{M}\tilde{\mathbf{Y}}''+\left\{\begin{array}{c}0\\ -\Omega^2 J_a\tilde{X}'_2\\ \Phi_3\left[\dfrac{Y'_3+\tilde{Y}'_3}{\sqrt{(X'_3+\tilde{X}'_3)^2+(Y'_3+\tilde{Y}'_3)^2}}-\dfrac{Y'_3}{\sqrt{X'^2_3+Y'^2_3}}\right]\\ \Phi_4\left[\dfrac{Y'_4+\tilde{Y}'_4}{\sqrt{(X'_4+\tilde{X}'_4)^2+(Y'_4+\tilde{Y}'_4)^2}}-\dfrac{Y'_4}{\sqrt{X'^2_4+Y'^2_4}}\right]\end{array}\right\}=0 \tag{13b}$$

Pre-multiplying Eqs. (13a) and (13b) by $\tilde{\mathbf{X}}'^{\mathrm{T}}$ and $\tilde{\mathbf{Y}}'^{\mathrm{T}}$, respectively, and summing them, one gets

$$\begin{aligned}&\sum_{i,j}K_{ij}(\tilde{X}_i\tilde{X}'_j+\tilde{Y}_i\tilde{Y}'_j)+2\Omega\sum_j D_{jj}(\tilde{X}'^2_j+\tilde{Y}'^2_j)+\Omega^2\sum_j M_{jj}(\tilde{X}'_j\tilde{X}''_j+\tilde{Y}'_j\tilde{Y}''_j)\\ &+\Phi_3\left[\frac{\tilde{X}'_3(X'_3+\tilde{X}'_3)+\tilde{Y}'_3(Y'_3+\tilde{Y}'_3)}{\sqrt{(X'_3+\tilde{X}'_3)^2+(Y'_3+\tilde{Y}'_3)^2}}-\frac{\tilde{X}'_3X'_3+\tilde{Y}'_3Y'_3}{\sqrt{X'^2_3+Y'^2_3}}\right]\\ &+\Phi_4\left[\frac{\tilde{X}'_4(X'_4+\tilde{X}'_4)+\tilde{Y}'_4(Y'_4+\tilde{Y}'_4)}{\sqrt{(X'_4+\tilde{X}'_4)^2+(Y'_4+\tilde{Y}'_4)^2}}-\frac{\tilde{X}'_4X'_4+\tilde{Y}'_4Y'_4}{\sqrt{X'^2_4+Y'^2_4}}\right]=0\end{aligned} \tag{14}$$

Indicating with $\mathbf{V}_j$ and $\tilde{\mathbf{V}}_j$ ($j=3$ or 4) the dimensionless velocity vectors of the supports, for the steady solution and for the perturbation, the factors of Φ_j inside square brackets can be written in the form $(\mathbf{V}_j+\tilde{\mathbf{V}}_j)\cdot\tilde{\mathbf{V}}_j/|\mathbf{V}_j+\tilde{\mathbf{V}}_j|-\mathbf{V}_j\cdot\tilde{\mathbf{V}}_j/|\mathbf{V}_j|$ and they represent the difference of the components of $\tilde{\mathbf{V}}_j$ along directions $\mathbf{V}_j+\tilde{\mathbf{V}}_j$ and $\mathbf{V}_j$. Indicating then the angle between $\mathbf{V}_j+\tilde{\mathbf{V}}_j$ and $\mathbf{V}_j$ with α_j (see Fig. 2), these components can be written as $|\mathbf{V}_j+\tilde{\mathbf{V}}_j|-|\mathbf{V}_j|\cos\alpha_j$ and $|\mathbf{V}_j+\tilde{\mathbf{V}}_j|\cos\alpha_j-|\mathbf{V}_j|$, so that their difference is $(|\mathbf{V}_j+\tilde{\mathbf{V}}_j|+|\mathbf{V}_j|)(1-\cos\alpha_j)$ and is always positive, unless $\alpha_j=0$, i.e. unless the two velocities $\mathbf{V}_j+\tilde{\mathbf{V}}_j$ and $\mathbf{V}_j$ are aligned and concordant. Nevertheless, in this case, the perturbation motion $(\tilde{\mathbf{X}},\tilde{\mathbf{Y}})$ would coincide with a natural motion by Eq. (13) and the support velocities could not be constantly aligned with the steady motion. Consequently, the dry friction terms of Eq. (14) are always positive, save at the alignment time instants.

Therefore the sum of the integrals of the elastic term and of the mass term of Eq. (14) is a convenient choice for a positive-definite Lyapunov function L (perturbation energy function):

$$L(\tilde{X},\tilde{X}',\tilde{Y},\tilde{Y}')=\frac{1}{2}\sum_{i,j}K_{ij}(\tilde{X}_i\tilde{X}_j+\tilde{Y}_i\tilde{Y}_j)+\frac{\Omega^2}{2}\sum_j M_{jj}\left(\tilde{X}'^2_j+\tilde{Y}'^2_j\right) \tag{15}$$

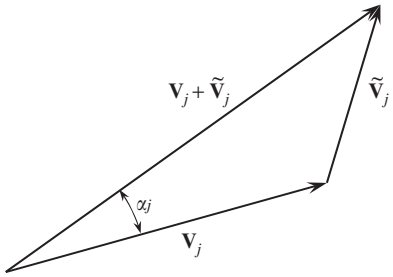

Fig. 2. Journal box velocities, $\mathbf{V}_j$ and $\tilde{\mathbf{V}}_j$, in the steady and the perturbed motions.

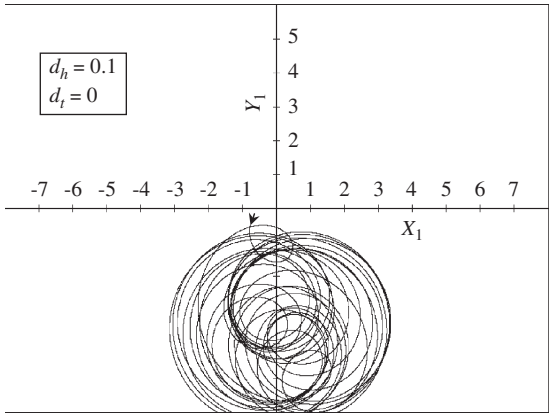

Fig. 3. Example of transient path of rotor centre in presence of shaft hysteresis. Viscous damping absent. Data: $K_3 = K_4 = 0.5$; $M_3 = M_4 = 0.5$; $J_d = 0.4$; $J_a = 0.2$; $L_3 = 0.4$; $d_r = 0$; $\Phi_3 = \Phi_4 = 1.5$; $G = 0.3$; $\Omega = 2$.

whose total derivative with respect to θ is negative along any solution trajectory by Eq. (14), even for vanishing viscous dissipation, giving thus the proof of the asymptotic stability of the steady motion.

This above stability proof holds also if one of the supports is motionless with an adhesive contact of the friction surfaces, while for both motionless supports, the stability of the system has to be considered either as orbital (in the sense of Lyapunov) in the absence of viscous resistance, or as asymptotic in its presence.

The stability proof no longer holds in the case of a hysteretic shaft material, where, as is well known, instability conditions may grow up above the first critical speed when the other external damping sources are not sufficient to counteract the hysteresis destabilizing effect. The condition of stability may be inspected, for example, by the small perturbation approach [16], which, owing to the nonlinearity inherent in the dry friction terms, involves linear differential equations with periodic coefficients, and hence the Floquet theory [22] may be applied as in [16]. Otherwise, for a more general control of the stability in the large, a numerical technique of the Runge–Kutta type may be applied, starting from random initial values of the variables and integrating the differential system as long as a sufficiently large number of rotor revolutions have been performed. Figs. 3 and 4 show the path of the rotor–shaft connection point O_1 for a supercritical example case in the presence of hysteresis, the first without and the second with external viscous damping, whose stabilizing influence is clearly visible in Fig. 4, where the trajectory approaches a stable circular attractor asymptotically. With the hypothesis of nearly ideal elasticity of the shaft material (d_h small), even the small environmental external damping always present in all rotor-support systems may be sufficient to quench the unstable trend due to hysteresis. For this purpose, also viscous dampers acting between the supports and the fixed frame could work very efficiently. In this case, the third and the fourth diagonal terms of matrix $\mathbf{D}$, which are zero in the present model, would not be so.

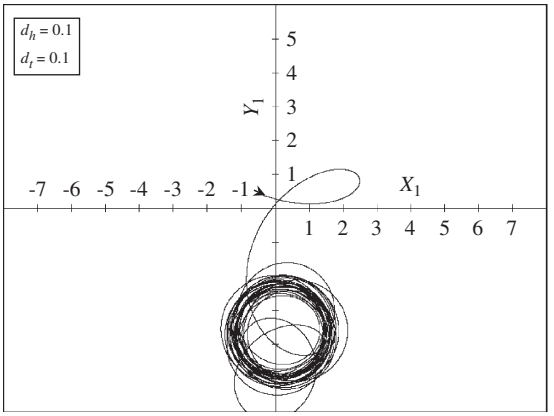

Fig. 4. Example of transient path of rotor centre in presence of shaft hysteresis. Viscous damping present. Data: $K_3 = K_4 = 0.5$; $M_3 = M_4 = 0.5$; $J_d = 0.4$; $J_a = 0.2$; $L_3 = 0.4$; $d_r = 0$; $\Phi_3 = \Phi_4 = 1.5$; $G = 0.3$; $\Omega = 2$.

5. Natural modes

The natural whirling speeds ω_n of the ideal system without unbalance and without viscous, hysteretic and Coulombian dissipation can be obtained by Eq. (9), putting $\mathbf{D} = \mathbf{H} = 0$, $\Phi_3 = \Phi_4 = 0$, multiplying by e, letting $e \to 0$ and replacing the products eW_j, which remain finite, with $eW_j = w_{j0}\exp(\mathrm{i}\lambda\theta)$, where $\lambda = \omega_n/\omega$:

$$[\mathbf{K} - \Omega_n^2 \mathbf{M}_g(\lambda)]\mathbf{w}_0 = 0 \tag{16}$$

Here, $\Omega_n = \lambda\Omega = \omega_n/\omega_c$ indicates the dimensionless whirling speed and $\mathbf{M}_g(\lambda)$ the "gyroscopic" diagonal mass matrix, whose elements are (1, J_d–J_a/λ, M_3, M_4). The eigenvalue problem defined by Eq. (16) can be easily worked out by solving the characteristic equation

$$\begin{vmatrix} K_{11} - \Omega_n^2 & K_{12} & K_{13} & K_{14} \\ K_{21} & K_{22} - \Omega_n^2(J_d - J_a/\lambda) & K_{23} & K_{24} \\ K_{31} & K_{32} & K_{33} - \Omega_n^2 M_3 & K_{34} \\ K_{41} & K_{42} & K_{43} & K_{44} - \Omega_n^2 M_4 \end{vmatrix} = 0 \tag{17}$$

for $1/\lambda$ in dependence on Ω_n^2, i.e.

$$\frac{1}{\lambda} = \frac{J_d}{J_a} - \frac{1}{\Omega_n^2 J_a}\left(K_{22} + \frac{K_{12}K_{12}^{(c)} + K_{32}K_{32}^{(c)} + K_{42}K_{42}^{(c)}}{K_{22}^{(c)}}\right) \tag{18}$$

where the $K_{ij}^{(c)}$'s are the cofactors of the coefficients $\ldots_{ij}$ in the determinant of Eq. (17), functions of Ω_n^2. This procedure permits tracing the plots of Ω_n, dimensionless precession speed, versus Ω, dimensionless angular speed of the shaft.

Figs. 5 and 6 show examples of these diagrams, the one for a hinged–hinged shaft case and the other for a clamped–free case, both for an oblate ellipsoid of inertia of the rotor ($J_d < J_a$) and for an elongated ellipsoid ($J_d > J_a$). Notice that the case of the cantilever shaft can be studied by the above equations dropping the terms with subscript 4 and expressing the stiffness coefficients suitably.

Similar to the fixed-support case, Eq. (18) indicates that there is a horizontal asymptote $\Omega_n = 0$, an inclined asymptote with slope $\lambda = \Omega_n/\Omega = J_a/J_d$ and three other couples of asymptotes parallel and symmetric with respect to the Ω-axis (only two couples for the clamped–free system), given by the roots of the equation $K_{22}^{(c)} = 0$, which is a cubic (quadratic) equation in Ω_n^2. The critical flexural speeds of the ideal system are given by the intersection of the straight line $\Omega_n = \Omega$ with these plots. They are four (three) in number if $J_a/J_d < 1$, due to the lower slope of the inclined asymptote in comparison with the bisector of the coordinate axes, otherwise they are three (two).

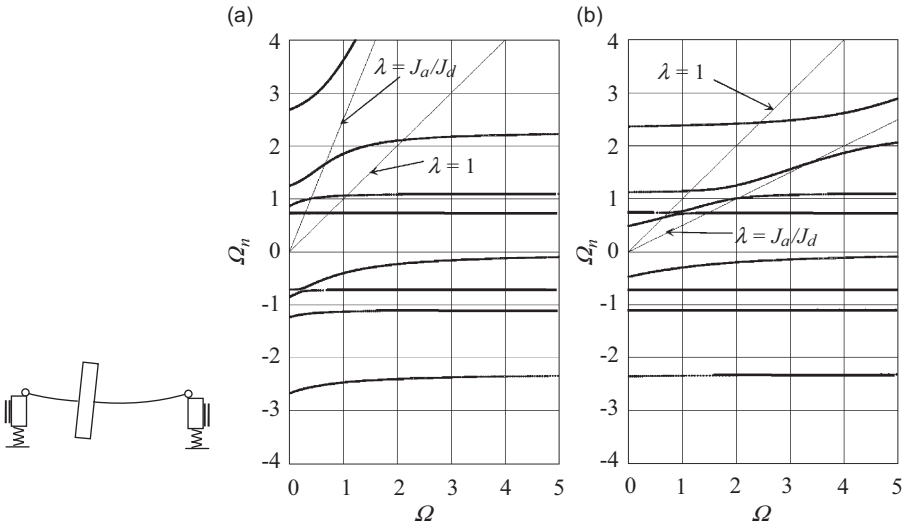

Fig. 5. Natural whirling modes for a hinged–hinged shaft. $L_3=0.3$. $K_3=K_4=1$; $M_3=M_4=1$; $J_a=0.25$. (a) $J_d=0.1$, oblate ellipsoid of inertia of rotor and (b) $J_d=0.5$, elongated ellipsoid of inertia of rotor.

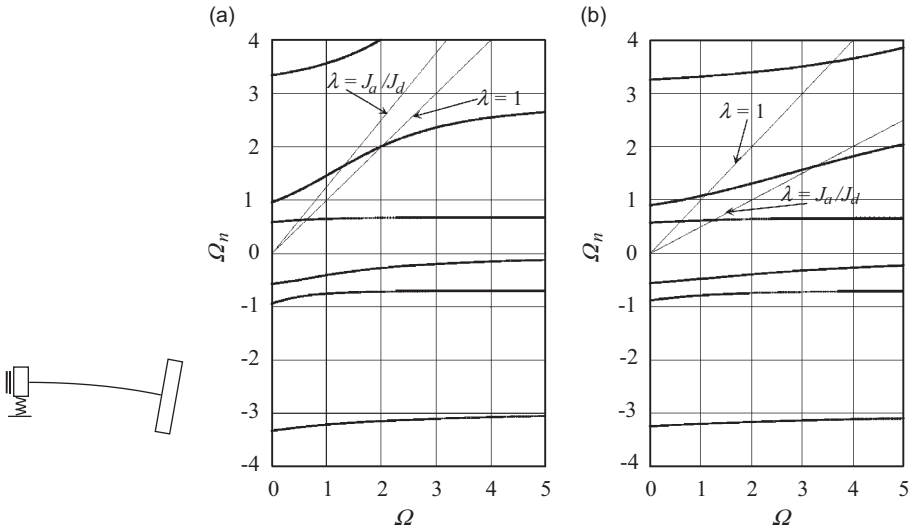

Fig. 6. Natural whirling modes for a cantilever shaft. $K_3=1$; $M_3=1$. (a) $J_a=0.5$, $J_d=0.4$, oblate ellipsoid of inertia of rotor and (b) $J_a=0.25$, $J_d=0.5$, elongated ellipsoid of inertia of rotor.

The diagrams show four (three) forward ($\Omega_n>0$) and four (three) backward precession motions ($\Omega_n<0$). They may grow up in transient condition, but die out in practice at the steady state.

6. Circular solution

The steady-state circular solution can be obtained in a straightforward manner. Putting $\mathbf{W}=\mathbf{W}_0\exp(i\theta)$, where $\mathbf{W}_0$ is the complex amplitude vector, and considering that the successive derivatives of $\mathbf{W}$ are given

by $\mathbf{W}^{(n)} = \mathbf{W}\exp(\mathrm{i}n\pi/2)$, Eq. (9) yields

$$[\mathbf{I} + 2\mathrm{i}\Omega\mathbf{AD} - \Omega^2\mathbf{A}\mathbf{M}_g(1)]\mathbf{W}_0 = \mathbf{Z}\mathbf{W}_0$$
$$= \mathbf{A}\left\{\Omega^2, 0, -\mathrm{i}\sigma_3\Phi_3\ \exp(\mathrm{i}\arg W_{0,3}) - (1-\sigma_3)\hat{\Phi}_{\mathrm{adh},3}, -\mathrm{i}\sigma_4\Phi_4\ \exp(\mathrm{i}\arg W_{0,4}) - (1-\sigma_4)\hat{\Phi}_{\mathrm{adh},4}\right\}^{\mathrm{T}} \quad (19)$$

where $\mathbf{I}$ is the identity matrix, $\mathbf{A}$ the flexibility matrix of Eq. (3) or (8a), $\mathbf{M}_g(1)$ is the gyroscopic mass matrix $\mathbf{M}_g(\lambda)$ of the previous section, calculated for $\lambda = 1$ and the notation $\mathbf{Z}$ has been introduced for brevity for the dynamical impedance matrix, which multiplies the unknown vector $\mathbf{W}_0$. Moreover, the terms $-\mathrm{i}\sigma_j\Phi_j$ and $-\hat{\Phi}_{\mathrm{adh},j}(1-\sigma_j)$ give the complex amplitudes of the dimensionless sliding forces and adhesion forces, respectively.

It is remarkable, though it was expected, that the hysteresis term has disappeared from Eq. (19), because the steady circular solution does not imply any shape change of the shaft deflection line in the rotating reference $O_3\xi_0\eta_0\zeta_0$ of Fig. 1. Thus, the hysteresis effect is just on the static part of the rotating shaft configuration and its destabilizing effect can be counteracted by the other dissipation sources.

Denoting by with $\mathbf{Z}_0$ the non-viscous impedance matrix ($\mathbf{Z}_0 = \mathbf{I} - \Omega^2\mathbf{A}\mathbf{M}_g(1)$), one can put, in order to facilitate the numerical inversion of the whole complex matrix $\mathbf{Z}$,

$$\mathbf{Z} = \mathbf{Z}_0 + 2\mathrm{i}\Omega\begin{bmatrix} d_tA_{11} & d_rA_{12} & 0 & 0 \\ d_tA_{21} & d_rA_{22} & 0 & 0 \\ d_tA_{31} & d_rA_{32} & 0 & 0 \\ d_tA_{41} & d_rA_{42} & 0 & 0 \end{bmatrix}$$
$$= \mathbf{Z}_0 + \mathbf{D}_t - \mathbf{D}_{t0} + \mathbf{D}_r - \mathbf{D}_{r0} + \mathbf{D}_{tr} - \mathbf{D}_{t0r} - \mathbf{D}_{tr0} + \mathbf{D}_{t0r0} \quad (20)$$

where

- $\mathbf{D}_t$ is obtained by $\mathbf{Z}_0$ replacing the first column by $\{2\mathrm{i}\Omega d_tA_{j1}\}$,
- $\mathbf{D}_{t0}$ is obtained by $\mathbf{D}_t$ replacing the first column by zeroes,
- $\mathbf{D}_r$ is obtained by $\mathbf{Z}_0$ replacing the second column by $\{2\mathrm{i}\Omega d_rA_{j2}\}$,
- $\mathbf{D}_{r0}$ is obtained by $\mathbf{D}_r$ replacing the second column by zeroes,
- $\mathbf{D}_{tr}$ is obtained by $\mathbf{Z}_0$ replacing the first column by $\{2\mathrm{i}\Omega d_tA_{j1}\}$ and the second column by $\{2\mathrm{i}\Omega d_rA_{j2}\}$,
- $\mathbf{D}_{t0r}$ is obtained by $\mathbf{D}_{tr}$ replacing the first column by zeroes,
- $\mathbf{D}_{tr0}$ is obtained by $\mathbf{D}_{tr}$ replacing the second column by zeroes,
- $\mathbf{D}_{t0r0}$ is obtained by $\mathbf{D}_{tr}$ replacing the first and second columns by zeroes.

It is easy to verify that Eq. (20) is identically satisfied and, moreover, the transpose cofactor matrix of the dynamical matrix $\mathbf{Z}$ is equal to the sum of the transpose cofactor matrices of the last member of Eq. (20).

Indicating generically with $\mathbf{D}^{(c)\mathrm{T}} = \mathbf{D}^{-1}\det\mathbf{D}$ the transpose cofactor matrix of any generic matrix $\mathbf{D}$, it is easy to recognize that $\mathbf{D}_t^{(c)\mathrm{T}}$ and $\mathbf{D}_{t0}^{(c)\mathrm{T}}$ have the same elements on the first row, while on the other three rows, all the elements of $\mathbf{D}_{t0}^{(c)\mathrm{T}}$ are null and all the elements of $\mathbf{D}_t^{(c)\mathrm{T}}$ have the common factor $2\mathrm{i}\Omega d_t$. Therefore, indicating by $\mathbf{D}_{\mathrm{real},t}$ the matrix obtainable by $\mathbf{D}_t$ dropping the imaginary factor $2\mathrm{i}\Omega d_t$ from the first column and indicating by $\mathbf{I}_1$ the identity matrix with a zero in the first diagonal place, the matrix difference $\mathbf{D}_t^{(c)\mathrm{T}} - \mathbf{D}_{t0}^{(c)\mathrm{T}}$ can be written as $2\mathrm{i}\Omega d_t\mathbf{I}_1\mathbf{D}_{\mathrm{real},t}^{(c)\mathrm{T}} = 2\mathrm{i}\Omega d_t\mathbf{D}_t^*$, where the first row is empty and for brevity $\mathbf{D}_t^* = \mathbf{I}_1\mathbf{D}_{\mathrm{real},t}^{(c)\mathrm{T}}$. Likewise, the difference $\mathbf{D}_r^{(c)\mathrm{T}} - \mathbf{D}_{r0}^{(c)\mathrm{T}}$ is given by $2\mathrm{i}\Omega d_r\mathbf{D}_r*$, where the second row is empty and $\mathbf{D}_r^* = \mathbf{I}_2\mathbf{D}_{\mathrm{real},r}^{(c)\mathrm{T}}$, $\mathbf{I}_2$ being the identity matrix with a zero in the second diagonal place. A quite similar reasoning leads to the result that $\mathbf{D}_{tr}^{(c)\mathrm{T}} - \mathbf{D}_{t0r}^{(c)\mathrm{T}} - \mathbf{D}_{tr0}^{(c)\mathrm{T}} = -4\Omega^2 d_td_r\mathbf{D}_{tr}^*$, where the first and the second rows are empty, and $\mathbf{D}_{tr}^* = \mathbf{I}_{12}\mathbf{D}_{\mathrm{real},tr}^{(c)\mathrm{T}}$, $\mathbf{I}_{12}$ being the identity matrix with zeroes in the first and second diagonal places. As regards the last matrix $\mathbf{D}_{t0r0}$ of Eq. (20), it is clear that $\mathbf{D}_{t0r0}^{(c)\mathrm{T}} \equiv 0$.

Since the determinant of the total dynamical matrix is equal to the sum of the determinants of the matrices at last hand of Eq. (20), where all matrices with zero subscripts have obviously null determinants, the inverse

of $\mathbf{Z}$ can be written in the following form, suitable for the numerical calculation, where the real and imaginary parts are well separated, both at the numerator and the denominator

$$\mathbf{Z}^{-1}=\frac{\mathbf{Z}_0^{(c)\mathrm{T}}-4\Omega^2 d_t d_r \mathbf{D}_{tr}^{*}+2\mathrm{i}\Omega(d_t\mathbf{D}_t^{*}+d_r\mathbf{D}_r^{*})}{\det\,\mathbf{Z}_0-4\Omega^2 d_t d_r\,\det\,\mathbf{D}_{\mathrm{real},tr}+2\mathrm{i}\Omega(d_t\,\det\,\mathbf{D}_{\mathrm{real},t}+d_r\,\det\,\mathbf{D}_{\mathrm{real},r})} \tag{21}$$

The steady circular solution of Eq. (19) can be obtained multiplying by $\mathbf{Z}^{-1}$ and putting $W_{0,j}=R_j\exp(-\mathrm{i}\gamma_j)$, where, for $j=1,3,4$, the R_j's are the orbital radii of the rotor and support paths, whilst R_2 is the rotor orbital slope. Splitting Eq. (19) into their real and imaginary parts, it is possible to write down eight scalar equations in the eight unknowns R_j and γ_j. In this regard, it is to be noticed that, in case of adhesion of any support ($\sigma_j=0$), the correspondent sliding term $-\mathrm{i}\,\Phi_j\exp(-\mathrm{i}\gamma_j)$ has to be replaced by the adhesive term $-\hat{\Phi}_{\mathrm{adh},j}$, whose modulus and argument are unknown, so that two new unknowns show up in place of γ_j, but, since the correspondent radius R_j vanishes, the mathematical model remains consistent. Therefore, replacing the exponential quantity $\exp(-\mathrm{i}\gamma_j)$ with a more general complex quantity $\hat{N}_j$, the modulus and the argument of $\hat{N}_j$ are 1 and $-\gamma_j$ for $R_j>0$, while they are both unknown for $R_j=0$, in which case the modulus $|\hat{N}_j|$ is equal in practice to the amplitude ratio of the adhesive force to the sliding force, as arguable by replacing $\hat{\Phi}_{\mathrm{adh},j}$ with $\mathrm{i}\Phi_j\hat{\Phi}_{\mathrm{adh},j}/(\mathrm{i}\Phi_j)$ into Eq. (19).

Using Eqs. (20) and (21), the inversion of the complex algebraic system (19) may be shown to lead to

$$\begin{aligned}
R_1\,\exp(-\mathrm{i}\gamma_1)&=c_{10}-\mathrm{i}c_{13}\hat{N}_3-\mathrm{i}c_{14}\hat{N}_4\\
R_2\,\exp(-\mathrm{i}\gamma_2)&=c_{20}-\mathrm{i}c_{23}\hat{N}_3-\mathrm{i}c_{24}\hat{N}_4\\
R_3\,\exp(-\mathrm{i}\gamma_3)&=c_{30}-\mathrm{i}c_{33}\hat{N}_3-\mathrm{i}c_{34}\hat{N}_4\\
R_4\,\exp(-\mathrm{i}\gamma_4)&=c_{40}-\mathrm{i}c_{43}\hat{N}_3-\mathrm{i}c_{44}\hat{N}_4
\end{aligned} \tag{22a,b,c,d}$$

where the coefficients $c_{ij}=c_{ij,r}+\mathrm{i}c_{ij,i}$ are complex in general, but become real in the absence of viscous dissipation ($c_{ij,i}=0$), and moreover they can be readily calculated by means of any matrix algebra software. The influence of dry friction on the system behaviour is condensed in the coefficients $\hat{N}_j$ of Eq. (22).

In the hypothesis of sliding contact of both supports, where $\exp(-\mathrm{i}\gamma_3)\equiv\hat{N}_3$ and $\exp(-\mathrm{i}\gamma_4)\equiv\hat{N}_4$, one has to solve Eqs. (22c, d) for the unknowns $\hat{N}_3$ and $\hat{N}_4$ (depending on R_3 and R_4):

$$\begin{aligned}
\hat{N}_3&=\frac{c_{30,r}R_4+n_{30,r}+\mathrm{i}(c_{30,i}R_4+n_{30,i})}{R_3R_4-(c_{44,i}R_3+c_{33,i}R_4)+d_{0,r}+\mathrm{i}(c_{44,r}R_3+c_{33,r}R_4+d_{0,i})}\\
\hat{N}_4&=\frac{c_{40,r}R_3+n_{40,r}+\mathrm{i}(c_{40,i}R_3+n_{40,i})}{R_3R_4-(c_{44,i}R_3+c_{33,i}R_4)+d_{0,r}+\mathrm{i}(c_{44,r}R_3+c_{33,r}R_4+d_{0,i})}
\end{aligned} \tag{23a,b}$$

where

$$\begin{aligned}
n_{30,r}&=c_{40,r}c_{34,i}+c_{40,i}c_{34,r}-c_{30,r}c_{44,i}-c_{30,i}c_{44,r}, & n_{30,i}&=c_{30,r}c_{44,r}-c_{30,i}c_{44,i}+c_{40,i}c_{34,i}-c_{40,r}c_{34,r}\\
n_{40,r}&=c_{30,r}c_{43,i}+c_{30,i}c_{43,r}-c_{40,r}c_{33,i}-c_{40,i}c_{33,r}, & n_{40,i}&=c_{40,r}c_{33,r}-c_{40,i}c_{33,i}+c_{30,i}c_{43,i}-c_{30,r}c_{43,r}\\
d_{0,r}&=c_{34,r}c_{43,r}-c_{34,i}c_{43,i}-c_{33,r}c_{44,r}+c_{33,i}c_{44,i}, & d_{0,i}&=c_{34,r}c_{43,i}+c_{34,i}c_{43,r}-c_{33,r}c_{44,i}-c_{33,i}c_{44,r}
\end{aligned}$$

Then the conditions $|\hat{N}_3|=|\hat{N}_4|=1$ give place to the double equation

$$\begin{aligned}
&R_4^2(c_{30,r}^2+c_{30,i}^2)+2R_4(c_{30,r}n_{30,r}+c_{30,i}n_{30,i})+(n_{30,r}^2+n_{30,i}^2)\\
&\quad=R_3^2(c_{40,r}^2+c_{40,i}^2)+2R_3(c_{40,r}n_{40,r}+c_{40,i}n_{40,i})+(n_{40,r}^2+n_{40,i}^2)\\
&\quad=[R_3R_4-(c_{44,i}R_3+c_{33,i}R_4)+d_{0,r}]^2+(c_{44,r}R_3+c_{33,r}R_4+d_{0,i})^2
\end{aligned} \tag{24a,b}$$

If one or both the supports are stuck, solutions (23a,b) are still valid, but the unitary conditions of the moduli no longer hold true.

For $R_3=0$, $R_4\neq0$ (adhesion of support 3), only $|\hat{N}_4|$ is unitary and one gets

$$(d_{0,r}-c_{33,i}R_4)^2+(d_{0,i}+c_{33,r}R_4)^2=n_{40,r}^2+n_{40,i}^2, \qquad \hat{N}_3=\frac{c_{30,r}R_4+n_{30,r}+\mathrm{i}(c_{30,i}R_4+n_{30,i})}{-c_{33,i}R_4+d_{0,r}+\mathrm{i}(c_{33,r}R_4+d_{0,i})} \tag{25a,b}$$

For $R_3 \neq 0$, $R_4 = 0$ (adhesion of support 4), only $|\hat{N}_3|$ is unitary and one gets

$$(d_{0,r} - c_{44,i}R_3)^2 + (d_{0,i} + c_{44,r}R_3)^2 = n_{30,r}^2 + n_{30,i}^2, \qquad \hat{N}_4 = \frac{c_{40,r}R_3 + n_{40,r} + \mathrm{i}(c_{40,i}R_3 + n_{40,i})}{-c_{44,i}R_3 + d_{0,r} + \mathrm{i}(c_{44,r}R_3 + d_{0,i})} \tag{26a,b}$$

For $R_3 = 0$, $R_4 = 0$ (adhesion of both supports), neither $|\hat{N}_3|$ nor $|\hat{N}_4|$ is equal to one and one gets

$$\hat{N}_3 = \frac{n_{30,r} + \mathrm{i}n_{30,i}}{d_{0,r} + \mathrm{i}d_{0,i}} \qquad \hat{N}_4 = \frac{n_{40,r} + \mathrm{i}n_{40,i}}{d_{0,r} + \mathrm{i}d_{0,i}} \tag{27a,b}$$

To sum up, in order to explore the rotor response to the unbalance throughout the whole angular speed range for fixed geometrical and mechanical parameters of the rotating machine, one must calculate the complex impedance matrix $\mathbf{Z}$ by Eq. (20) for each speed Ω and then invert it by Eq. (21), to get the coefficients c_{ij} of Eq. (22).

Then, assuming firstly sliding conditions for both the journal boxes, Eq. (24) are to be applied for the calculation of R_3 and R_4. Each of the three members appearing in Eq. (24) can be considered as a function $f(R_3, R_4)$ of R_3 and R_4, representing a surface in the space (R_3, R_4, f), and in particular, the first two functions represent two parabolic cylinders with generatrices parallel to the R_3-axis and to the R_4-axis respectively, while the third one represents a fourth-order surface spreading above the plane (R_3, R_4) without touching it. Looking for a possible common intersection point of these three surfaces, which might not necessarily exist however, and proceeding by elimination of either R_3 or R_4, one would be lead to solve an eight degree algebraic equation and therefore, some technique of the trial and error type must be necessarily used.

If Eq. (24) do not give real positive roots for R_3 and R_4, one or both the journal boxes are in an adhesive state and the possible roots of the two quadratic Eqs. (25a) and (26a) are firstly to be searched. In the case of only one positive root, either $R_4 > 0$ or $R_3 > 0$, one has to ascribe the stick state to the other support and the modulus of the corresponding complex number $\hat{N}_j$, calculated either by Eq. (25b) or by Eq. (26b), gives the amplitude ratio of the static friction force to the sliding force. If no positive root is found, there are stick conditions on both supports and the moduli of the numbers $\hat{N}_j$ of Eq. (27) give their static-to-sliding friction force amplitude ratios. In the case of two positive roots on the contrary, $R_4 > 0$ of Eq. (25a) and $R_3 > 0$ of Eq. (26a), two possible whirling motion may develop, one with stuck state of the support 3 and the other with stuck state of 4. Nevertheless, it is possible to verify by the obtainable results that one of such two motions implies static friction forces that are greater than the sliding force, while the other implies lower static forces, which in particular become equal to the sliding force, on varying the speed Ω, at the transition from the stick to the slip state. Of course, the first possibility should be checked by comparison with the static friction limit

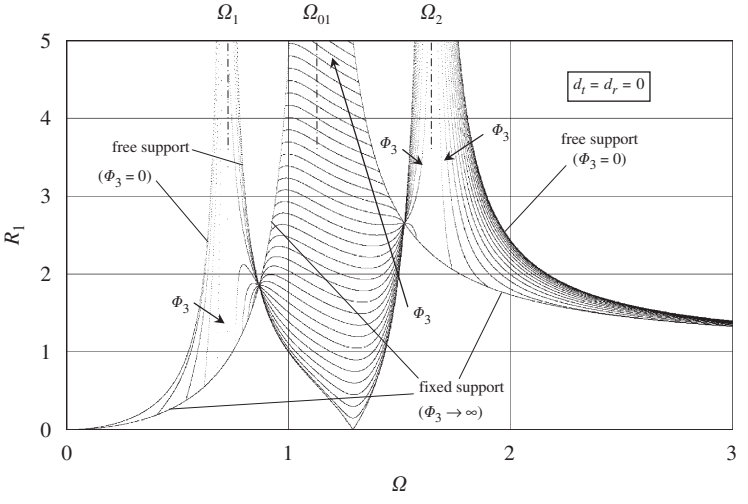

Fig. 7. Orbital radius of rotor, scaled by e, for a clamped–free shaft. Viscous damping absent. $\Phi_3 = 0, 0.2, 0.4, 0.6, 0.8, \ldots$ (increasingly in the arrow direction); $K_3 = 2$; $M_3 = 2$; $J_a - J_d = 0.1$; Ω_{0j} and Ω_j are the critical speeds of fixed-support and free-support systems.

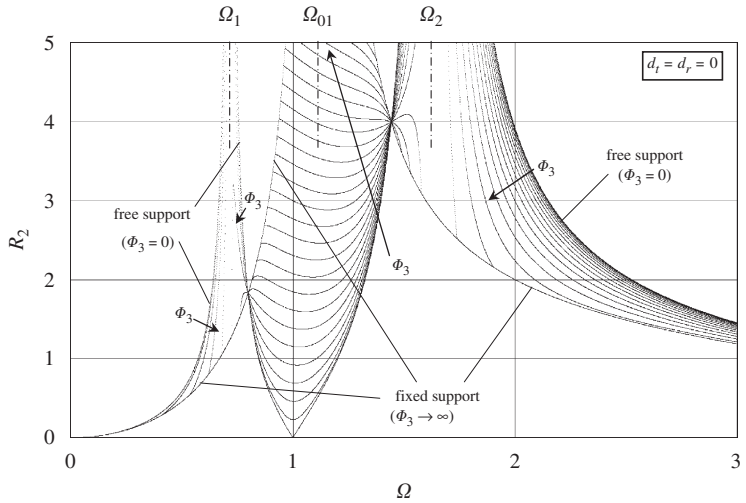

Fig. 8. Orbital slope of rotor, scaled by e/l, for a clamped–free shaft. Viscous damping absent. $\Phi_3 = 0, 0.2, 0.4, 0.6, 0.8, \ldots$ (increasingly in the arrow direction); $K_3 = 2$; $M_3 = 2$; $J_a - J_d = 0.1$; Ω_{0j} and Ω_j are the critical speeds of fixed-support and free-support systems.

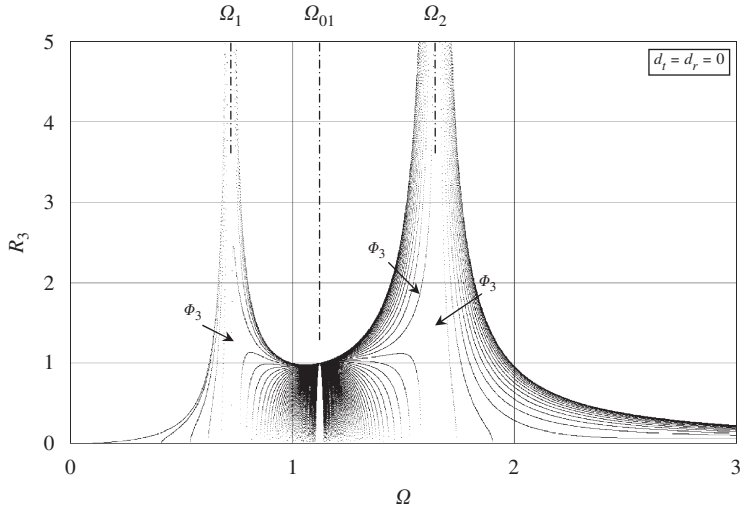

Fig. 9. Orbital radius of journal box, scaled by e, for a clamped–free shaft. Viscous damping absent. $\Phi_3 = 0, 0.2, 0.4, 0.6, 0.8, \ldots$ (increasingly in the arrow direction); $K_3 = 2$; $M_3 = 2$; $J_a - J_d = 0.1$; Ω_{0j} and Ω_j are the critical speeds of fixed-support and free-support systems.

and, in any case, could not be attained when arriving from a sliding state at the stick state by means of a gradual speed variation. Therefore, only the second type of whirling motion is here accepted as feasible.

Clearly, in the case of a cantilever shaft, the field of possible situations is more limited, as the sizes of the matrices descend to 3×3 and there is only one friction contact that may become stuck.

Figs. 7–9 show the diagrams of the orbital radius and slope of the rotor and of the path radius of the support, as functions of angular speed, for an example case of a rotor which is not subject to viscous dissipation and is mounted at the end of a cantilever shaft, for different levels of the friction force on the dry friction surface (the friction force increases in the direction of arrows). The figures include also the limit cases of zero and infinite friction force and reported are also the critical speeds for these limit cases (two-mass frictionless system: $\Phi_3 = 0$; fixed-support system: $\Phi_3 \to \infty$).

Starting from zero friction force and increasing its level gradually, adhesive ranges show up in the high- and low-speed fields, where the rotor response coincides with the fixed-support case ($\Phi_3 \to \infty$), and the extents of these adhesive regions spread towards the speed mid-range on increasing the friction force Φ_3. Moreover, the rotor motion amplitude in the sliding range grows gradually with the friction level in the neighbourhood of the critical speed of the fixed-support system, until it becomes infinitely large. At the same time, the range of the support motion shrinks on increasing the friction level until it becomes a vertical segment of unit height placed at the fixed-support critical speed (Fig. 9). Between these two extremes conditions, zero friction with sliding support and infinite friction with stuck support, an optimum condition has to be searched, choosing a compromise solution where the critical speeds of the frictionless free-support system are cut off by the adhesive state while the motion amplitude remains reasonably moderate near the critical speed of the fixed-support system, by letting the support slide.

In the hypothesis of no viscous dissipation, the solution can be obtained straightforwardly in closed form. Accounting for Eq. (8a), reducing to 3×3 the sizes of the algebraic system (19) and assuming that the support is sliding, it is possible to write the motion equations in the following form:

$$\begin{aligned}
&\left[1-\Omega^2\left(1+\frac{1}{K_3}\right)\right][1+R_1\,\exp(-\mathrm{i}\gamma_1)]-\frac{3}{2}\Omega^2(J_d-J_a)R_2\,\exp(-\mathrm{i}\gamma_2)-\Omega^2\frac{M_3}{K_3}R_3\,\exp(-\mathrm{i}\gamma_3)\\
&\quad=1-\frac{\Phi_3\,\exp(-\mathrm{i}\gamma_3)}{K_3}\\
&-\frac{3}{2}\Omega^2[1+R_1\,\exp(-\mathrm{i}\gamma_1)]+[1-3\Omega^2(J_d-J_a)]R_2\,\exp(-\mathrm{i}\gamma_2)=0\\
&-\frac{\Omega^2}{K_3}[1+R_1\,\exp(-\mathrm{i}\gamma_1)]+\left(1-\Omega^2\frac{M_3}{K_3}\right)R_3\,\exp(-\mathrm{i}\gamma_3)=-\frac{\Phi_3\,\exp(-\mathrm{i}\gamma_3)}{K_3}
\end{aligned}\tag{28a,b,c}$$

where the matrix of the coefficients on the left-hand side is the 3×3 non-viscous dynamical matrix $[Z]_0$. Indicating with $Z^{(c)}_{0,ij}$ the cofactors of $Z_{0,ij}$ and solving for $R_3\exp(-\mathrm{i}\gamma_3)$, one gets

$$\left[R_3\,\det\,\mathbf{Z}_0+\mathrm{i}\frac{\Phi_3}{K_3}(Z^{(c)}_{0,13}+Z^{(c)}_{0,33})\right]\exp(-\mathrm{i}\gamma_3)=Z^{(c)}_{0,13}\tag{29}$$

whence observing that $\det\mathbf{Z}_0=Z^{(c)}_{0,33}-M_3\Omega^2(Z^{(c)}_{0,13}+Z^{(c)}_{0,33})/K_3$, one derives

$$R_3^2=\frac{Z^{(c)2}_{0,13}-(\Phi_3/K_3)^2(Z^{(c)}_{0,13}+Z^{(c)}_{0,33})^2}{\left[Z^{(c)}_{0,33}-(M_3\Omega^2(Z^{(c)}_{0,13}+Z^{(c)}_{0,33}))/K_3\right]^2},\quad \gamma_3=\arctan\left\{\frac{\Phi_3(Z^{(c)}_{0,13}+Z^{(c)}_{0,33})}{R_3\left[K_3Z^{(c)}_{0,33}-M_3\Omega^2(Z^{(c)}_{0,13}+Z^{(c)}_{0,33})\right]}\right\}\tag{30}$$

For $Z^{(c)2}_{0,13}>(\Phi_3/K_3)^2(Z^{(c)}_{0,13}+Z^{(c)}_{0,33})^2$, there is sliding at the support, otherwise there is adhesion with $R_3=0$, $\gamma_3=\pm\pi/2$ and $|\hat{\Phi}_3|=|K_3Z^{(c)}_{0,13}/(Z^{(c)}_{0,13}+Z^{(c)}_{0,33})|$ by Eq. (29).

After calculating R_3 and γ_3, the unknowns R_1 and γ_1 can be easily obtained by Eq. (28c) and then R_2 and γ_2 by Eq. (28b), though they are not reported here for brevity, as their expressions are somehow long.

Some few other remarks about the diagrams of Figs. 7–9 are to be made. It is interesting that, in the hypothesis of no dissipation at all ($\Phi_3=0$), the solution of the algebraic system (28) furnishes a unitary value for R_1 and a zero value for the rotor slope R_2 for $\Omega^2=K_3/M_3$, as clearly appears in Figs. 7 and 8, where $K_3/M_3=1$. On the other hand, the orbital radius R_1 vanishes when the product $(1-\Omega^2M_3/K_3)[1-3\Omega^2(J_d-J_a)]$ is equal to the determinant of the system (28), which condition gives rise to a quadratic equation for Ω^2, with only one positive root in particular for $J_a-J_d>0$. This root appears in Fig. 7 and may be verified to correspond to the critical speed of the undamped system when the additional constraint $R_1=0$ is also imposed, which is, as is well known, a general property of the forced oscillations of multi-degree-of-freedom systems. No zeroes of R_1 or R_2 can be found on the contrary for $\Phi_3>0$, whilst a number of common intersection points of various curves for different Φ_3 values are clearly observable in Figs. 7 and 8. They can be obtained by cancelling the factors of Φ_3 in the expressions of R_1 and R_2, which conditions give rise to a quartic and a cubic algebraic equations, respectively.

In order to recognize the effect of viscous damping, Figs. 10–12 refer to the same data of Figs. 7–9, but add some viscous dissipation. There are no longer resonance discontinuities in the diagrams and the curves show

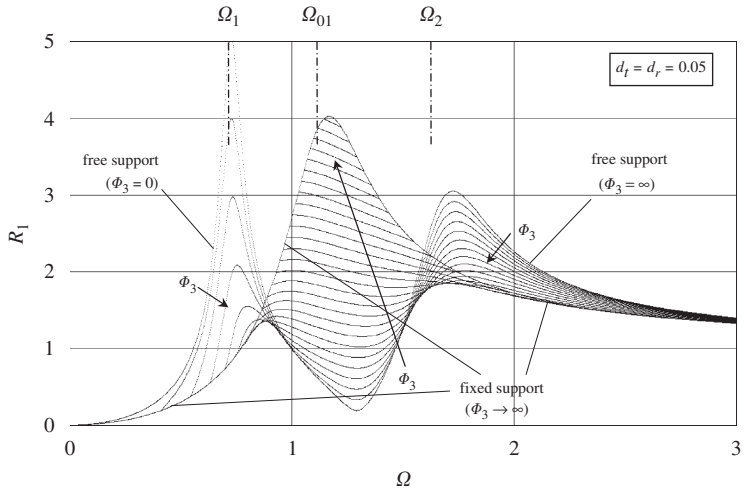

Fig. 10. Orbital radius of rotor, scaled by e, for a clamped–free shaft. Viscous damping present. $\Phi_3 = 0, 0.2, 0.4, 0.6, 0.8, \ldots$ (increasingly in the arrow direction); $K_3 = 2$; $M_3 = 2$; J_a–$J_d = 0.1$; Ω_{0j} and Ω_j are the critical speeds of fixed-support and free-support systems.

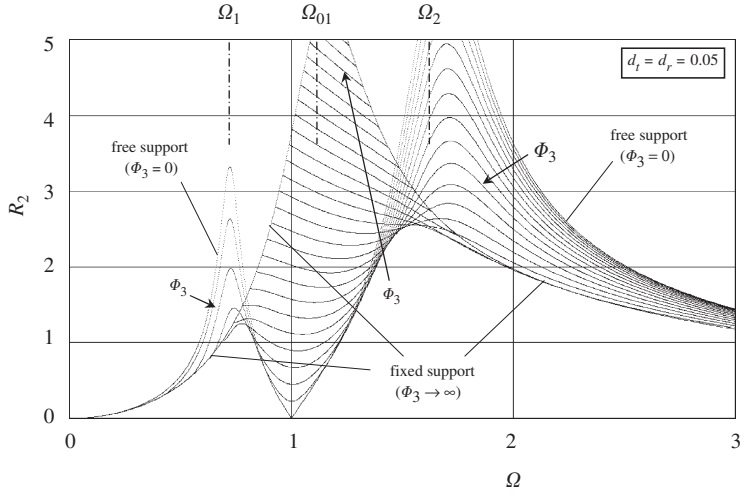

Fig. 11. Orbital slope of rotor, scaled by e/l, for a clamped–free shaft. Viscous damping present. $\Phi_3 = 0, 0.2, 0.4, 0.6, 0.8, \ldots$ (increasingly in the arrow direction); $K_3 = 2$; $M_3 = 2$; J_a–$J_d = 0.1$; Ω_{0j} and Ω_j are the critical speeds of fixed-support and free-support systems.

lower amplitudes as a whole, with no common intersection points. The orbital radius R_1 does not vanish for any speed Ω in the absence of dry friction, while the slope R_2 does still vanish as previously for $\Omega^2 = K_3/M_3$, as easily verifiable by the system equations.

The cases of shafts on two resilient supports are much more varied. Here, only the non-viscous configuration will be considered, as we are mainly interested in the effects of dry friction.

Figs. 13–16 show the speed response for an example case of a hinged–hinged shaft, for constant sliding friction resistance on support 4 and several friction levels on support 3. Similar conclusions can be drawn as for the clamped–free shaft, though the results are a little more complex. The stuck regions of support 3 originate in the low- and high-speed ranges and spread toward the mid-range on increasing the dry friction level Φ_3, permitting to cut off the critical speeds of the undamped system, while the whirl amplitude remains quite moderate in the slip range. The two supports may be in the slip or the stick state either separately of simultaneously depending on the rotating speed and different values of the two friction forces. Remarks

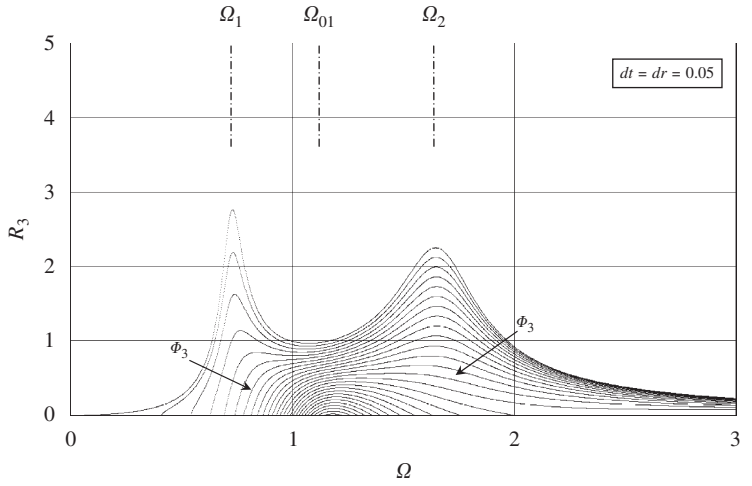

Fig. 12. Orbital radius of journal box, scaled by e, for a clamped–free shaft. Viscous damping present. $\Phi_3 = 0$, 0.2, 0.4, 0.6, 0.8, … (increasingly in the arrow direction); $K_3 = 2$; $M_3 = 2$; J_a–$J_d = 0.1$; Ω_{0j} and Ω_j are the critical speeds of fixed-support and free-support systems.

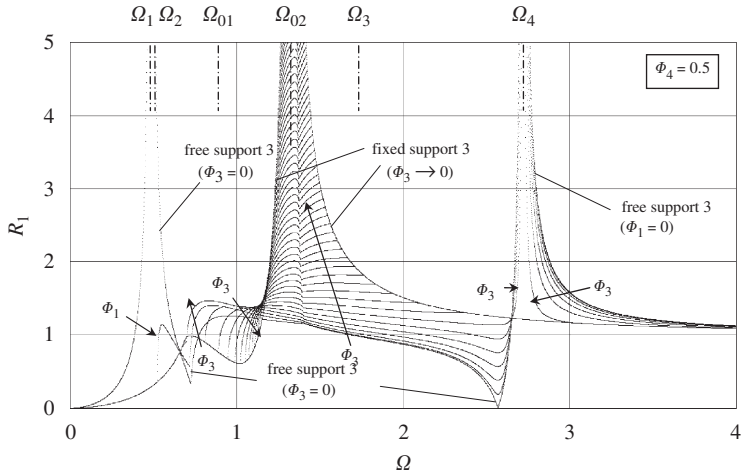

Fig. 13. Orbital radius of rotor, scaled by e, for a hinged–hinged shaft. Viscous damping absent. $\Phi_3 = 0$, 0.2, 0.4, 0.6, 0.8, … (increasingly in the arrow direction) $d_t = d_r = 0$; $K_3 = K_4 = 0.2$; $M_3 = M_4 = 0.2$; J_d–$J_a = 0.2$; $L_3 = 0.4$; Ω_{0j} and Ω_j are the critical speeds of fixed-support and free-support systems.

similar to those for cantilever shaft can be made about the zeroes of the undamped system responses and the intersection points of various plots for different Φ_3, though such results are obtainable now by solving higher-degree algebraic equations. The strange changes of the speed response shape for the orbital radius and the slope of the rotor, on increasing the friction level, are due to the closeness of some critical speeds to each other and to the complicated alternation of slip and stick states of the one and the other journal box, as shown in Figs. 15 and 16.

7. Optimization of the dry friction damping system

In the light of the previous results, it may appear desirable to look for an optimized configuration of the support system and for the best level of friction forces, in order to reduce the overall drawbacks of the whirling motion. This search requires fixing some specific optimization weights for the amplitudes of various motions

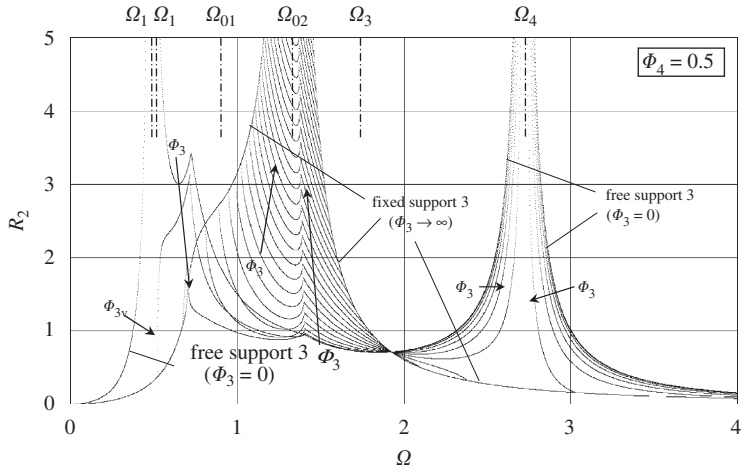

Fig. 14. Orbital slope of rotor, scaled by e/l, for a hinged–hinged shaft. Viscous damping absent. $\Phi_3 = 0, 0.2, 0.4, 0.6, 0.8, \ldots$ (increasingly in the arrow direction) $d_t = d_r = 0$; $K_3 = K_4 = 0.2$; $M_3 = M_4 = 0.2$; J_d–$J_a = 0.2$; $L_3 = 0.4$; Ω_{0j} and Ω_j are the critical speeds of fixed-support and free-support systems.

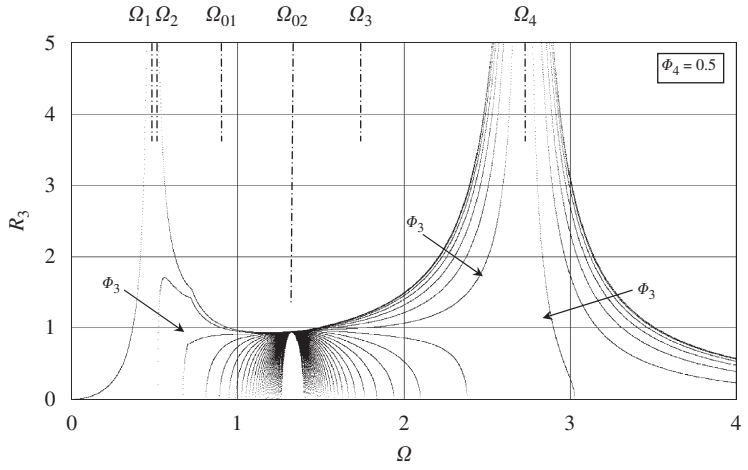

Fig. 15. Orbital radius of back journal box, scaled by e, for a hinged–hinged shaft. Viscous damping absent. $\Phi_3 = 0, 0.2, 0.4, 0.6, 0.8, \ldots$ (increasingly in the arrow direction) $d_t = d_r = 0$; $K_3 = K_4 = 0.2$; $M_3 = M_4 = 0.2$; J_d–$J_a = 0.2$; $L_3 = 0.4$; Ω_{0j} and Ω_j are the critical speeds of fixed-support and free-support systems.

produced by the rotor unbalance, i.e. for the orbital radii of the rotor and the supports and for the conical attitude of the rotor axis, with the aim for example of minimizing the maximum value of the weighted average of their amplitude throughout the speed range.

Of course, one should check that the slip interval does not contain the critical speeds of the rotating machine on mobile no-friction supports, as the addition of the dry friction resistance could not quench such resonances unless the adhesion limits are exceeded and the characteristic frequencies of the new constrained system have become different. Nevertheless, it is to be said that the presence of some extra dissipation forces acting on the rotor, for example of the viscous kind, might attenuate these resonance peaks.

The dry friction dampers should act in practice as automatic clutches controlled by the angular speed, blocking the support motion when some critical speed of the undamped system is expected and releasing them on the contrary when the critical speeds of the fixed-support system are to be feared. This can be obtained, for given inertia of the rotor and journal boxes, and for given stiffness of the shaft and the suspension spring, by

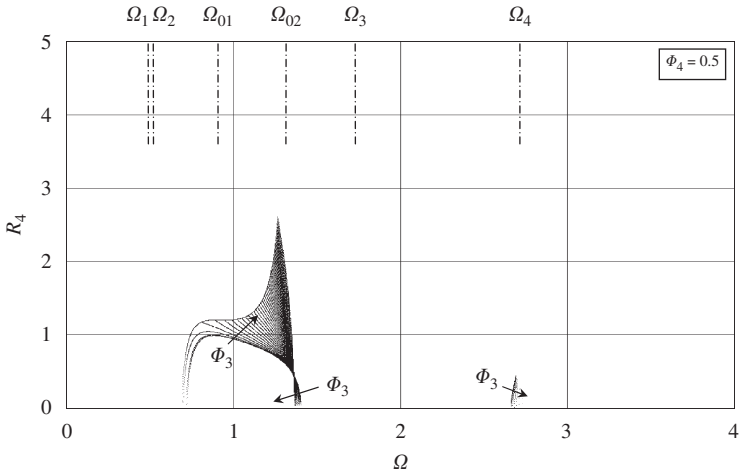

Fig. 16. Orbital radius of front journal box, scaled by e, for a hinged-hinged shaft. Viscous damping absent. $\Phi_3 = 0, 0.2, 0.4, 0.6, 0.8, \ldots$ (increasingly in the arrow direction) $d_t = d_r = 0$; $K_3 = K_4 = 0.2$; $M_3 = M_4 = 0.2$; J_d–$J_a = 0.2$; $L_3 = 0.4$; Ω_{0j} and Ω_j are the critical speeds of fixed-support and free-support systems.

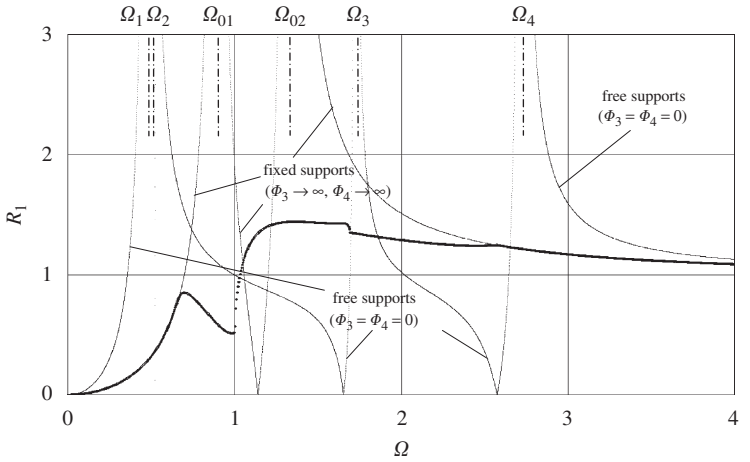

Fig. 17. Optimized orbital radius of rotor (thicker line), scaled by e, for a hinged–hinged shaft. Viscous damping absent. $w_1 = 0.3$; $w_2 = 0.3$; $w_3 = 0.2$; $w_4 = 0.2$; $\Phi_3 = 1.3160156$; $\Phi_4 = 0.39335938$; $R_{1,\max.} = 1.4395974$; $d_t = d_r = 0$; $K_3 = K_4 = 0.2$; $M_3 = M_4 = 0.2$; J_d–$J_a = 0.2$; $L_3 = 0.4$; Ω_{0j} and Ω_j are the critical speeds of fixed-support and free-support systems.

suitably tuning the values of the closure forces on the one and the other support, in order to produce the most convenient friction resistance to their motion.

This search can be carried out numerically, for example by some method of the gradient type applied to the two variables Φ_3 and Φ_4, or else, more simply, by varying one of such variables at a time and spanning the critical speed range at each step by the techniques described in the previous sections. In this procedure, the step size has to be reduced, e.g. quartered, in the close neighbourhood of the local minimum of an assumed criterion function, which can be defined for example by the above weighted average of the whirling amplitudes.

Figs. 17–20 show the optimized speed response of the rotor (R_1, R_2) and the supports (R_4, R_4) for an example case with hinged–hinged bearings and no viscous damping, assuming the four weight parameters $w_1 = 0.3$, $w_2 = 0.3$, $w_3 = 0.2$, $w_4 = 0.2$. The rotor amplitude curves for the fixed–fixed-support system and floating–floating support system in absence of dissipation are also shown, together with their asymptotes.

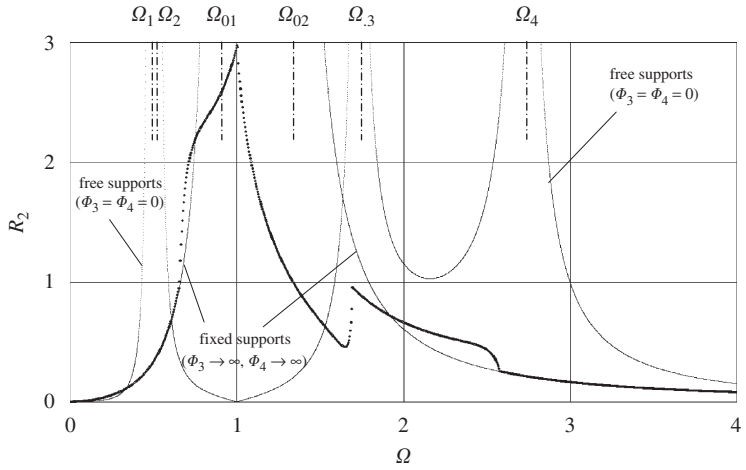

Fig. 18. Optimized orbital slope of rotor (thicker line), scaled by e/l, for a hinged–hinged shaft. Viscous damping absent. $w_1 = 0.3$; $w_2 = 0.3$; $w_3 = 0.2$; $w_4 = 0.2$; $\Phi_3 = 1.3160156$; $\Phi_4 = 0.39335938$; $R_{2,\max.} = 2.9740073$, $d_t = d_r = 0$; $K_3 = K_4 = 0.2$; $M_3 = M_4 = 0.2$; J_d–$J_a = 0.2$; $L_3 = 0.4$; Ω_{0j} and Ω_j are the critical speeds of fixed-support and free-support systems.

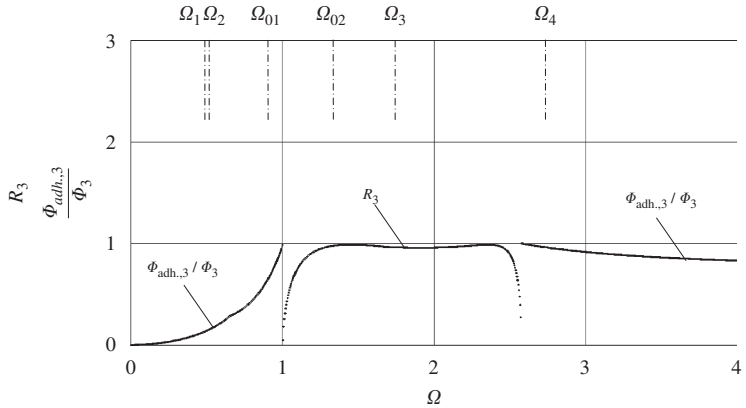

Fig. 19. Optimized orbital radius of back journal box, scaled by e, for a hinged–hinged shaft. Viscous damping absent. $w_1 = 0.3$; $w_2 = 0.3$; $w_3 = 0.2$; $w_4 = 0.2$; $\Phi_3 = 1.3160156$; $\Phi_4 = 0.39335938$; $R_{3,\max.} = 0.9873647$; $d_t = d_r = 0$; $K_3 = K_4 = 0.2$; $M_3 = M_4 = 0.2$; J_d–$J_a = 0.2$; $L_3 = 0.4$; Ω_{0j} and Ω_j are the critical speeds of fixed-support and free-support systems.

The maximum whirl amplitude in the slip range is also indicated, showing the good efficiency of the dry friction dampers in cutting all critical speeds by their adhesive state and in restraining the whirl amplitude in the remaining range. Figs. 19 and 20 show also the adhesive force level in the stuck range.

The optimization process can be carried out in a more systematic way, looking for the best combinations of the couple of numbers Φ_3 and Φ_4 in correspondence of various degrees of asymmetry of the rotating system ($L_4 \neq L_3$) and tracing the diagrams of the optimized parameters in dependence on the rotor distance L_3 from one support. This is shown in Figs. 21 and 22 for the two cases of an elongated and an oblate ellipsoid of inertia of the rotor, whose diagrams may give a very helpful tool to choose the most suitable axial load and produce the best friction force. In the second case (oblate ellipsoid), the support 4 turns out to be in an adhesive state when the rotor dissymmetry is large (i.e. when L_3 is small) and the corresponding minimum adhesive force $\Phi_{\text{adh.,}4}$ to prevent the support motion, at incipient sliding conditions, is calculated and indicated in this range. Nevertheless, it is to be said that it is clearly more convenient to block definitively such a support in that operative field. The non-smoothness of the curves in some points is due to the change of the critical speed values when varying the system parameters.

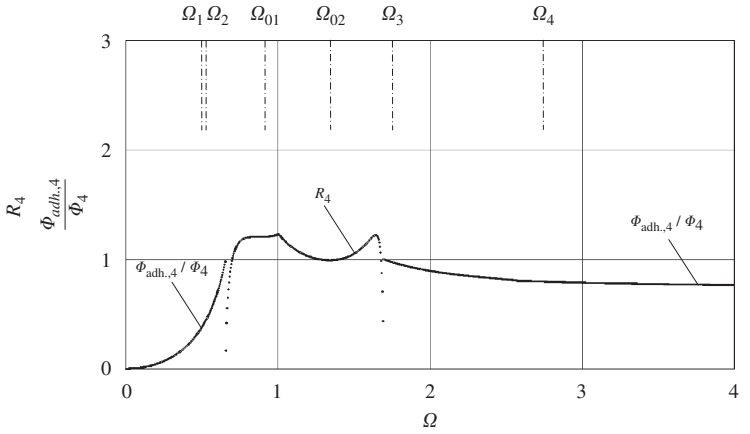

Fig. 20. Optimized orbital radius of front journal box, scaled by e, for a hinged–hinged shaft. Viscous damping absent. $w_1 = 0.3$; $w_2 = 0.3$; $w_3 = 0.2$; $w_4 = 0.2$; $\Phi_3 = 1.3160156$; $\Phi_4 = 0.39335938$; $R_{4,\max.} = 1.2297435$; $d_t = d_r = 0$; $K_3 = K_4 = 0.2$; $M_3 = M_4 = 0.2$; J_d–$J_a = 0.2$; $L_3 = 0.4$; Ω_{0j} and Ω_j are the critical speeds of fixed-support and free-support systems.

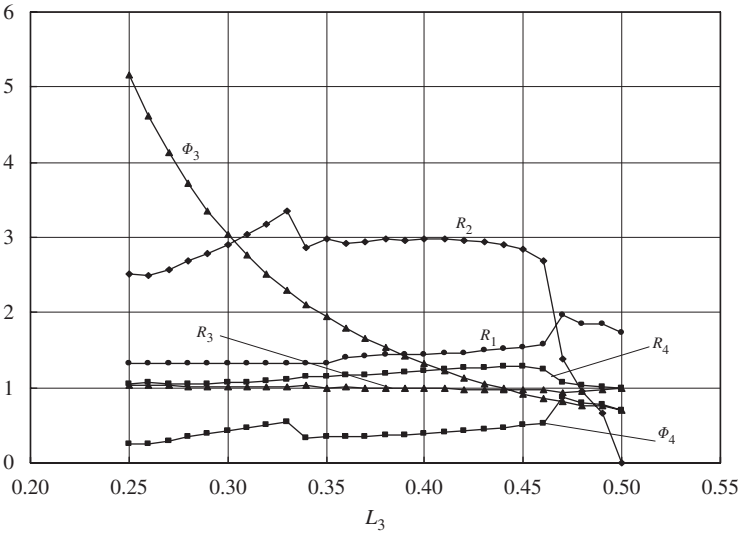

Fig. 21. Optimized rotor parameters, for a hinged–hinged shaft. $w_1 = 0.3$; $w_2 = 0.3$; $w_3 = 0.2$; $w_4 = 0.2$, $d_t = d_r = 0$; $K_3 = K_4 = 0.2$; $M_3 = M_4 = 0.2$; J_d–$J_a = 0.2$ (elongated ellipsoid of inertia of rotor).

Fig. 23 shows the optimized parameters for the case of a cantilever shaft with a rotor at the free end, in dependence on the oblate degree J_a–J_d of the inertia ellipsoid and similar considerations can be made. Moreover, it must be pointed out here that, in the case of an elongated ellipsoid of inertia (J_a–$J_d < 0$), the three critical speeds to be cancelled are quite separated from each other and the optimization results turn out to be much poorer than in Fig. 23.

8. Conclusion

The present analysis wants to propose a new technique to quench the unbalance effects and the whirling motions in rotating machinery, and its particular efficiency in the neighbourhood of the critical flexural speeds is noteworthy. This practice consists in suspending the shaft journal boxes on suitable elastic supports, creating front and rear flat rubbing surfaces, orthogonal to the shaft axis, and assigning to these dry friction

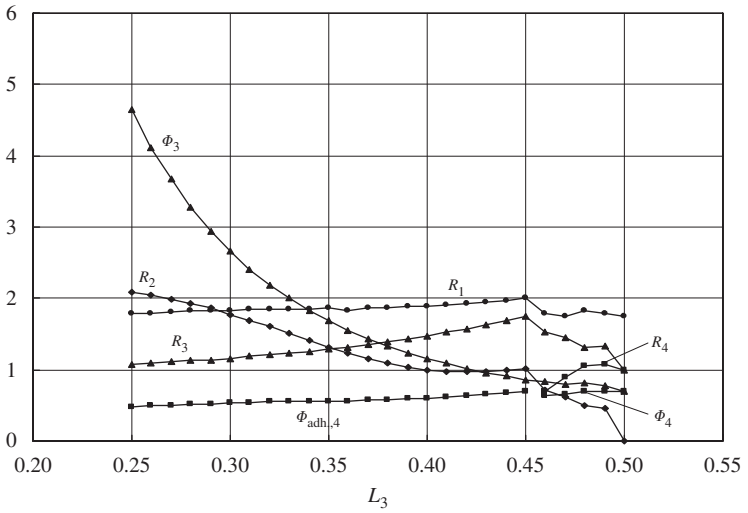

Fig. 22. Optimized rotor parameters, for a hinged–hinged shaft. $w_1 = 0.3$; $w_2 = 0.3$; $w_3 = 0.2$; $w_4 = 0.2$, $d_t = d_r = 0$; $K_3 = K_4 = 0.2$; $M_3 = M_4 = 0.2$; J_a–$J_d = 0.2$ (oblate ellipsoid of inertia of rotor).

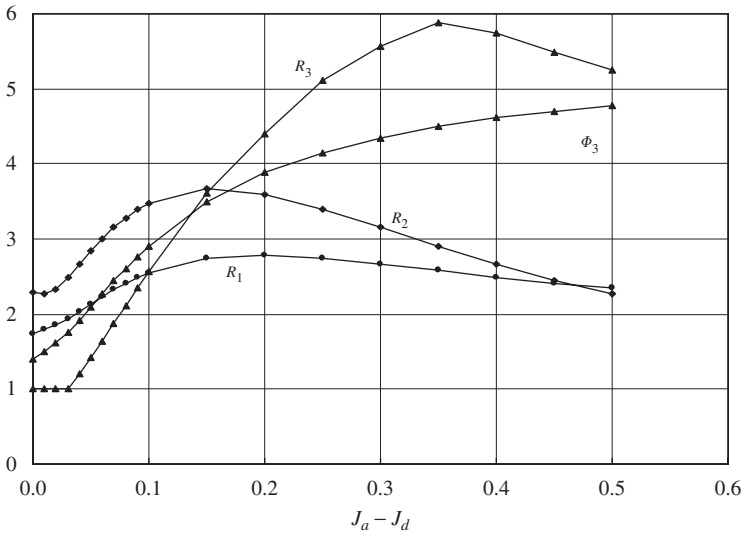

Fig. 23. Optimized rotor parameters, for a clamped–free shaft. $w_1 = 0.4$; $w_2 = 0.4$; $w_3 = 0.2$, $d_t = d_r = 0$; $K_3 = 0.4$; $M_3 = 0.4$.

devices the task of restraining all critical whirl motions that arise. The wear compensation of the slip surfaces does not create any problem, as it can be achieved automatically in the long run by the use of proper spring loading systems to fasten the sliding contacts.

Adhesion conditions occur between such friction surfaces in some parts of the speed range, where the rotor behaves thus in the conventional way. Actually, the best use of the dry friction suspensions can be achieved by confining the multi-degree-of-freedom critical speeds in these stuck ranges and letting the journal boxes slide in the range that would be critical for the fixed-support system. The dry friction dampers act then like automatic clutches that block or release the journal boxes depending on the working requirements.

In practice, the most convenient condition of the suspension system for the usual working is the adhesive state, where is neither relevant energy dissipation nor heat production, while the sliding motion should be activated only occasionally, to prevent and damp the critical speed of the simple rotor on fixed supports.

Another significant advantage of the dry friction dampers consists in the possibility of minimizing the whirling motion also in the slip range by a proper choice of the friction level as a function of suspension-to-shaft stiffness ratio and on support-to-rotor mass ratio.

Future development of the present analysis will consist in an experimental validation of the theoretical results on a small scale rotor model with adjustable friction forces on the supports.

References

[1] J. Jiang, H. Ulbrich, Stability analysis of sliding whirl in a nonlinear Jeffcott rotor with cross-coupling stiffness coefficients, *Nonlinear Dynamics* 24-3 (2001) 269–283.

[2] D.W. Childs, Rub-induced parametric excitation in rotors, *ASME Journal of Mechanical Design* 101 (1979) 640–644.

[3] D.W. Childs, Fractional-frequency rotor motion due to non-symmetric clearance effects, *ASME Journal of Engineering for Power* 104 (1982) 533–541.

[4] J.Y. Zhao, I.W. Linnett, L.J. McLean, Stability and bifurcation of unbalanced response of a squeeze film damped flexible rotor, *ASME Journal of Tribology* 116 (1994) 361–368.

[5] M.D. Rabinowitz, E.J. Hahn, Stability of squeeze-film damper supported flexible rotors, *ASME Journal of Engineering Power* 99 (1977) 545–551.

[6] M.D. Rabinowitz, E.J. Hahn, Steady-state performance of squeeze-film damper supported flexible rotors, *ASME Journal of Engineering Power* 99 (1977) 552–558.

[7] R.G. Kirk, E.J. Gunter, The effect of support flexibility and damping on the synchronous response of a single-mass flexible rotor, *ASME Journal of Engineering for Industry* 94 (1972) 221–232.

[8] R.G. Kirk, E.J. Gunter, Effect of support flexibility and damping on the dynamic response of a single-mass flexible rotor in elastic bearings, NASA CR-2083, July 1972.

[9] Z. Guo, R.G. Kirk, Theoretical study on instability boundary of rotor-hydrodynamic bearing systems: part I—Jeffcott rotor with external damping, *ASME Journal of Vibration and Acoustics* 125 (2003) 417–422.

[10] Z. Guo, R.G. Kirk, Theoretical study on instability boundary of rotor-hydrodynamic bearing systems: part II—rotor with external flexible damped support, *ASME Journal of Vibration and Acoustics* 125 (2003) 423–426.

[11] O. Montagnier, Ch. Hochard, Dynamic instability of supercritical driveshafts mounted on dissipative supports—effects of viscous and hysteretic internal damping, *Journal of Sound and Vibration* 305 (2007) 378–400.

[12] M. Aleyaasin, M. Ebrahimi, R. Whalley, Vibration analysis of distributed-lumped rotor systems, *Computer Methods in Applied Mechanics and Engineering* 189-2 (2000) 545–559.

[13] L.X. Liu, C.J. Teo, A.H. Epstein, Z.S. Spakovszky, Hydrostatic gas journal bearings for micro-turbomachinery, *Journal of Vibration and Acoustics* 127-2 (2005) 157–164.

[14] J.H. Song, D. Kim, Foil gas bearing with compression springs: analyses and experiments, *Journal of Tribology* 129-3 (3) (2007) 628–639.

[15] X. Zhu, L. San Andrés, Rotordynamic performance of flexure pivot hydrostatic gas bearings for oil-free turbomachinery, *Journal of Engineering for Gas Turbines and Power* 129-4 (2007) 1020–1027.

[16] F. Sorge, Rotor whirl damping by dry friction suspension systems, in: ECOTRIB 2007, European Conference on Tribology, Ljubljana, Slovenija, 12–15/06/2007, to be printed on MECCANICA, Springer, doi:10.1007/s11012-008-9134-6.

[17] R.G. Kirk, H. Hornschuch, Bearing and housing assembly, US Patent no. 4119375, October 10, 1978.

[18] D.C. Moringiello, S.H. Dallmann, Friction damper, US Patent no. 4337982, July 6, 1982.

[19] S.H. Crandall, Rotating and reciprocating machines, in: W. Flügge (Ed.), *Handbook of Engineering Mechanics*, McGraw-Hill, New York, USA, 1962.

[20] G. Diana, F. Cheli, *Dinamica e Vibrazioni dei Sistemi Meccanici (in Italian)*, Vol. 2, UTET Libreria, Torino, Italy, 1993.

[21] H.L. Wettergren, On the behavior of material damping due to multi-frequency excitation, *Journal of Sound and Vibration* 206 (1997) 725–735.

[22] A.H. Nayfeh, D.T. Mook, *Nonlinear Oscillations*, Wiley, New York, USA, 1979.